Appendix

Supplementary material for

The molecular products and biogeochemical significance of lipid photooxidation in West Antarctic surface waters

James R. Collins[a,b,*,1], Helen F. Fredricks[a], Jeff S. Bowman[c,2], Collin P. Ward[a], Carly Moreno[d], Krista Longnecker[a], Adrian Marchetti[d], Colleen M. Hansel[a], Hugh W. Ducklow[c], and Benjamin A. S. Van Mooy[a,*]

[a] Department of Marine Chemistry and Geochemistry, Woods Hole Oceanographic Institution, Woods Hole, MA 02543, USA
[b] MIT/WHOI Joint Program in Oceanography/Applied Ocean Science and Engineering, Woods Hole, MA 02543, USA
[c] Division of Biology and Paleo Environment, Lamont-Doherty Earth Observatory, Columbia University, Palisades, NY 10964, USA
[d] Department of Marine Sciences, University of North Carolina at Chapel Hill, Chapel Hill, NC 27599, USA

* Corresponding authors. *E-mail addresses:* james.r.collins@aya.yale.edu (James R. Collins), bvanmooy@whoi.edu (Benjamin A. S. Van Mooy).
[1] Present address: School of Oceanography and eScience Institute, University of Washington, Seattle, WA 98195, USA.
[2] Present address: Scripps Institution of Oceanography, University of California, San Diego, La Jolla, CA 92093, USA

Supplementary methodological details

A.1. Liposome photooxidation experiments

In the experiments, different combinations of phosphatidylcholine (PC) liposomes (Table A1) were incubated under natural sunlight to simulate the heterogeneous distribution of lipids found in natural membranes.

A.1.1. Preparation of liposomes

Liposomes are frequently used as structural analogs for membrane lipids (Wagner et al., 1994) in studies of lipid function and oxidation in both plant (e.g., Zhou et al., 2009) and human (e.g., Thomas et al., 2010) cells. For this study, an Avanti Mini-Extruder and seven species of synthetic phosphatidylcholine containing fatty acid moieties of varying unsaturation and chain length (full list, Table A1; molecular structures, Fig. A2) were obtained from Avanti Polar Lipids, Inc. (Alabaster, AL, USA). To improve the yield during the extruding process, the liposome suspensions used in the experiments were prepared from lipid films rather than from the simple dry lipid mixture recommended by the manufacturer. Detailed protocols for preparation of both films and liposomes have been published online and may be cited by DOI at https://doi.org/10.17504/protocols.io.haub2ew.

To prepare the films, known quantities of each lipid dissolved in chloroform (approx. 200 µL) were dispensed into 20 mL precombusted, round-bottomed, screw-top glass vials using a solvent-washed glass syringe. The chloroform was then evaporated under a constant stream of nitrogen gas while the vial was revolved continuously by hand around its major axis. By gradual evaporation of the chloroform in this manner, the lipid was deposited as a thin film along the inside wall of each vial. Residual chloroform was removed via vacuum centrifugation (30 minutes), the vials flushed with argon, and screw-top threads sealed with Teflon (PTFE) film. The vials were then capped and stored until needed (in all instances, < 2 months) at –20°C. The final quantity of lipid in each tube ranged from 500-2000 µg, depending on the species. Fresh liposomes were extruded from these films 1-2 hours before the start of each experiment according to a modified version of the manufacturer protocol. Briefly, for each lipid to be evaluated, a film was retrieved from cold storage and hydrated with 500 µL of a buffer solution containing 260 mM NaCl and 50 mM Tris (both reagent grade, Fisher Scientific, USA). The tube was then incubated for one hour at 60°C while subjected to gentle agitation. Using the Avanti Mini-Extruder, liposomes were then extruded from the lipid suspension by forcing the suspension multiple times through a 0.2 µm polycarbonate membrane. The extruder was maintained at 60-70°C by means of a hot plate. The protocol was repeated for as many lipids as required. Extruder components and syringes were rinsed between preparation of each batch of liposomes and a new membrane was used for each lipid. Based on concentrations of PC 22:6, 22:6 observed in $t = 0$ samples from the experiment for which we present

results in Fig. 4 and Table 1, we recovered 80.5 % of our starting lipid film as liposomes (t = 0 concentration, 1108 ± 125 pmol mL^{-1}; calculated concentration based on known mass of lipid film, 1376.1 pmol mL^{-1}).

A.1.2. Design and conduct of experiments

For each of the five experiments, a different combination of these liposomes (Table A1) was dispensed into a precombusted glass beaker fresh natural seawater filtered to either 0.2 or 0.7 μm ("- het. bact." and "+ het. bact." treatments respectively). Raw seawater used for both experimental matrixes was collected from the nearby harbor within an hour of the start of each experiment using tubing was flushed with 5 % hydrochloric acid. By filtering to 0.2 μm, we endeavored to exclude phytoplankton and heterotrophic bacteria while retaining dissolved organic matter. By contrast, the 0.7 μm-filtered matrix allowed us to evaluate the interaction between heterotrophic bacteria and UVR exposure in the presence of the liposomes; in these samples, we sought to retain a large fraction of the heterotrophic bacterial community but exclude the majority of large-celled eukaryotic phytoplankton.

A sufficient number of fused quartz glass incubation vessels (34.5 mL; Technical Glass Products, Painesville Twp., Ohio, USA) were then filled with the liposome-seawater suspension(s) to permit evaluation in triplicate at several time points of the light-exposed, + UVR treatment and, in the case of the 20 Nov. and 14 Dec. experiments, the - and + het. bact. treatments. Parallel incubations were conducted in vials of standard borosilicate laboratory glass (40 mL EPA vials of usable vol. 42 mL; Fisher Scientific, USA). The transmission spectrum of the borosilicate glass was nearly indistinguishable from the fused quartz at wavelengths > 320 nm (Fig. A1). To eliminate headspace when liposome suspensions were dispensed into the treatment vials, all vials were filled to slightly overflowing. The mouths of the vials were then covered with PTFE film prior to stoppering (quartz vials) or securing with screw caps (borosilicate vials). Black electrical tape was used to further seal the outsides of the stoppers or screw caps to ensure vials did not inadvertently open during incubation in the aquarium.

To simulate surface-layer conditions in the adjacent coastal ocean, incubations were conducted in a large, outdoor, green-bottomed aquarium at a water depth of 0.6 m. The aquarium was left open to the sky for the duration of each experiment. The Palmer Station seawater intake system was used to circulate fresh seawater through the aquarium at a rate sufficient to gently agitate the incubation vessels; the rate of circulation also served to maintain the water at a constant temperature. Total exposure times in the experiments ranged from 8.2 to 12.4 hours. Although we kept the incubation vessels as close to the center of the aquarium as possible, some minor shading of the samples might have occurred during the early mornings when the zenith angle was low and incoming radiation fluxes were small. Vials were placed in

the aquarium at least one vial length away from each other (15 cm) to minimize interactions between samples.

A.1.3. Treatment of samples from liposome experiments

Samples were transferred at predesignated timepoints during each experiment to precombusted., 200 mL glass separatory funnels. 30 µL of a synthetic IP-DAG (dinitrophenyl-phosphatidylethanolamine, or DNP-PE; Avanti Polar Lipids, Inc., Alabaster, AL, USA) was immediately added at known concentration as an internal standard. 20 mL dichloromethane (HPLC grade; Sigma-Aldrich) was then added, followed by 50 µL of 45.4 mM butylated hydroxytoluene (BHT; 99.8 %, Acros Organics) in HPLC-grade methanol (CHROMASOLV for HPLC; Sigma-Aldrich), thereby achieving an antioxidant concentration of 0.0025% (w/v) in the organic phase (Yao et al., 2008). The funnel was then stoppered and mixed vigorously three times; phases were allowed to separate briefly between mixing. The organic phase (ca. 20 mL) was then collected into a precombusted glass vial and reduced in volume to approx. 1.5 mL using a nitrogen blowdown system. The final extract was transferred to a precombusted HPLC vial, topped with argon, and then stored at –80°C until ready for analysis.

A.1.4. Malondialdehyde assay kit

The assay for malondialdehyde (MDA) was carried out according to the manufacturer protocol for tissue/cell samples using 400 µL sample, 300 µL of the provided lysis buffer, and 6 µL BHT (Lipid Peroxidation/MDA Assay Kit ab118970; Abcam Inc., Cambridge, UK). A 510/535 nm excitation/emission filter pair was used for fluorometric detection and quantification of the MDA-thiobarbituric acid (TBA) adduct.

A.1.5. Enzyme assay protocol and interactive script for rate determination

Assays for the bacterial exoenzymes lipase, alkaline phosphatase, α-D-glucosidase, and L-Leucine-4-methylcoumaryl-7-amide, or leu-MCA, were conducted as described in Edwards et al. (2011). Briefly, pre-prepared 96-well plates containing the substrates were inoculated with aliquots of sample from each treatment; the plates were incubated in darkness at the same temperature as the water in the aquarium. The hydrolysis of these substrates and the attendant release of the free fluorophores 4-methylumbelliferone and 7-amino-4-methylcoumarin was monitored over time using a Tecan Infinite F200 Pro plate reader. External standard curves were used to convert fluorescence values to concentration units; enzyme hydrolysis rates were then calculated by linear regression from the observed changes in concentration. A more detailed protocol and interactive MATLAB script for calculation of hydrolysis rates from raw fluorescence data are available at https://github.com/jamesrco/ExoenzymeHydroCalc

A.2. Acquisition and analysis of irradiance data

A.2.1. Data collected with the Jaz spectrometer

A.2.1.1. Time-series measurements during the liposome photooxidation experiments

During the experiments, *in situ* measurements with the Jaz instrument were made in the on-deck aquarium at the same 0.6 m depth as the incubation vessels using an upward-facing plane irradiance cosine corrector (180° field of view) and 5 or 10 m fiber optic cables that had been factory calibrated for absolute irradiance measurements from 210-850 nm. Irradiances were recorded at 1 min. intervals.

A.2.1.2. Depth profiles in Arthur Harbor

Profiles were made at Station B, a 75 m deep sampling location about 1 km offshore, occupied twice weekly during the austral summer as part the Palmer Long Term Ecological Research (PAL-LTER) study (Fig. 1b). Surface-corrected irradiances from depths immediately below the sea surface to 8 m were used to calculate a series of Napierian wavelength-dependent downwelling attenuation coefficients, $K_d(\lambda)$, for wavelengths from 320-700 nm, according to:

$$I_z(\lambda) = I_{0-}(\lambda)e^{-K_d(\lambda)z} \qquad \text{(A.1)}$$

where $I_z(\lambda)$ is the spectral irradiance at depth z and $I_{0-}(\lambda)$ is the spectral irradiance just below the sea surface. Due the low signal-to-noise ratio in our *in situ* irradiance observations at wavelengths < 320 nm, we estimated $K_d(\lambda)$ for these wavelengths from an exponential model fit to the adjacent data (Fig. A3).

To achieve minimum boat shadow while making the profile measurements, the light sensor (cosine corrector) and 10 m fiber optic cable were streamed away from the small boat using a counterweighted lowering frame in a direction that was both to windward and toward the sun. The frame was designed to maintain the sensor's vertical orientation toward the sea surface. During data acquisition, the boat was allowed to drift downwind from the measurement location to a suitable stand-off distance. Depth was monitored using an attached LAT 1000 Series pressure and temperature sensor (Lotek Wireless Inc., Newmarket, ON, Canada). Spectra were obtained at 16 depths from 0 to 8 m on days when few or no clouds were present. The profile data presented in Fig. A3 (from which we made the estimates of $K_d(\lambda)$ used in the lipid photooxidation calculations) were collected between 11:07 and 11:11 a.m. local time (GMT-3) on 15 December 2015 at PAL-LTER Station B; the solar zenith angle was 46.1°. While the Jaz sensor was deployed at depth, we made series of concurrent surface irradiance measurements with a LI-COR PAR sensor (model LI-193SA; LI-COR Biosciences, Lincoln, NE, USA); these were used to correct the depth profile spectra for changes in incident light intensity (due, e.g., to variations in cloud cover) that occurred between measurements. Eq. A.1 was solved 14 times at each wavelength to estimate $K_d(\lambda)$; we used the mean value for each wavelength in our subsequent calculations (Fig. A3; Table A3). The associated uncertainties were assimilated in the Monte Carlo error analysis. Because these $K_d(\lambda)$ are based on irradiance data collected only within the mixed layer, they

should be used with caution if applied to the rest of the water column. Subsequent measurements with a more advanced profiling instrument, described below, were used to confirm the accuracy of the $K_d(\lambda)$ at select wavelengths.

A.2.2. Depth profiles with the C-OPS instrument

Recognizing that we could not precisely monitor the attitude of the light sensor during the Jaz deployments, we reoccupied PAL-LTER Station B during a subsequent field season with a more advanced C-OPS profiling instrument (Biospherical Instruments Inc., San Diego, CA, USA). Irradiance data were acquired on 16 November 2017 at 18 wavelengths from 0 to 65 m at an effective vertical resolution of 4 mm. Data were subsequently controlled for pitch, roll, and upcasting according to Brosnan (2015) and Morrow et al. (2010). Eq. A.1 was then solved 1,052 times at each wavelength to estimate $K_d(\lambda)$. While we were unable to directly compare the Jaz and C-OPS in simultaneous deployments, the $K_d(\lambda)$ we estimated from the 2017 C-OPS profile agreed generally with those we estimated from the Jaz data collected at the same location two years earlier (Fig. A3).

A.2.3. Mathematical conversion of irradiance data

Where necessary for apparent quantum yield (AQY) calculations (main text, Section 2.6), we converted downwelling irradiances to wavelength-specific photon irradiances ($E_{n,\mathrm{p}}(\lambda)$, in units of μmol photons m^{-2} s^{-1}) using the equation

$$E_{n,\mathrm{p}}(\lambda) = I(\lambda) \times \lambda \times 0.836 \times 10^{-2} \qquad \text{(A.2)}$$

where λ is a given wavelength in nm, $I(\lambda)$ is the irradiance in W m^{-2}, and the additional numerical coefficients are used to effect necessary conversions via Planck's equation and Avogadro's number. Incident irradiances ($I_{0+}(\lambda)$) were converted to below-surface irradiances ($I_{0-}(\lambda)$) according to

$$I_{0-}(\lambda) = I_{0+}(\lambda)(1 - \rho(\lambda)) \qquad \text{(A.3)}$$

where $\rho(\lambda)$ is the fraction of light reflected back at the sea surface. $\rho(\lambda)$ was estimated for each irradiance observation from the solar zenith angle (θ_z) according to the relationship of Kirk (2011)

$$\rho(\lambda) = 5.43 \times 10^{-5}(1.115^{\theta_z}) + 2.03 \times 10^{-2} \qquad \text{(A.4)}$$

θ_z were computed using the R package RAtmosphere (Biavati, 2014).

A.2.4. Confirmation of calculated irradiances using chemical actinometry

A.2.4.1. Methodological details

Because it can be difficult to determine the optical pathlength in a curved vessel (Vähätalo et al., 2000), we conducted a follow-up experiment in 2017 to compare irradiances calculated from the *in situ* spectrophotometer data (Eq. 2, term under integral sign) to those measured directly in quartz glass vials using nitrite and nitrate-based chemical actinometers (Jankowski et al., 1999; D. J. Kieber et al., 2007).

The response bandwidths of the two actinometers were 330-380 and 311-333 nm, respectively. In the experiment, which was conducted on 14 November 2017, vials containing the actinometer solutions were incubated in triplicate for 2.6 h in the same outdoor aquarium used for the liposome experiments. The solar zenith angle at the experiment midpoint (local noon) was 47.2°. The tank temperature was maintained at –1°C; as a precaution against freezing, the actinometer solutions were made up in 0.7 M sodium chloride, as described in D. J. Kieber et al. (2007). The quartz vials containing the nitrite actinometer solution were sheathed in 4 mil Mylar D (polyethylene terephthalate) film; the mean transmissivity of the film over the response bandwidth (330-380 nm) and the transmissivity at the nitrite absorbance maximum (355 nm) were both 0.69.

A.2.4.2. Results

The irradiance we measured using the Mylar D-wrapped nitrite actinometer (20.5 ± 0.8 μmol photons cm^{-2}; mean ± SD of n = 3) was not significantly different from the integrated irradiance we estimated from the *in situ* Jaz data for the 330-380 nm spectral band (19.9 μmol photons cm^{-2}). By comparison, the irradiance we measured using the nitrate actinometer (2.6 ± 0.2 μmol photons cm^{-2}) was less than the irradiance we estimated for the 311-333 nm band (4.6 μmol photons cm^{-2}). These results suggest the *in situ* spectrophotometer provided accurate estimates of irradiance across a wide swath of the UVA spectrum despite underestimating fluxes in the narrower 311-333 nm band, which was less relevant to our work. This pattern was consistent with previous findings for a similar incubation system in which curved glass vials were used (D. J. Kieber et al., 2007).

A.3. Benchtop lipid and seawater absorbance measurements

A.3.1. Methodological details

Wavelength-specific absorbances of various PC lipid standards (Fig. A4) and surface seawater samples from Arthur Harbor (Fig. A5) were measured in the laboratory using a dual-path UV-visible spectrophotometer (Thermo Nicolet Evolution 300; ThermoFisher Scientific). Spectrophotometer data were obtained as decadic absorbances ($A(\lambda)$; dimensionless) using 100 mm quartz cuvettes. HPLC-grade methanol and 0.2 μm-filtered oligotrophic ocean seawater (collected from 50 m at the Bermuda-Atlantic Time Series site, 32° 10' N, 64° 30' W) were used as references for the lipid standards and Arthur Harbor seawater samples, respectively. Absorbance spectra of the standards (Fig. A4a,b) were used to calculate wavelength-specific molar decadic absorption coefficients ($\varepsilon_i(\lambda)$, in units of M^{-1} cm^{-1}; Fig. A4c) according to the equation

$$\varepsilon_i(\lambda) = \frac{A_i(\lambda)}{C_i \times \ell} \qquad \text{(A.5)}$$

where $A_i(\lambda)$ is the measured decadic absorbance at wavelength λ, ℓ is the pathlength (10 cm), and C_i is the concentration of the relevant analyte (liposome standard) in units of mol L^{-1}. Where necessary, these $\varepsilon_i(\lambda)$ were converted to Napierian coefficients ($\kappa_i(\lambda)$, in units of M^{-1} cm^{-1}) by multiplying by a factor of ln 10. Decadic absorbance spectra of the seawater samples ($A_{SW}(\lambda)$) were used to calculate wavelength-specific linear Napierian absorption coefficients ($\alpha_{SW}(\lambda)$, in units of m^{-1}; Fig. A5) according to:

$$\alpha_{SW}(\lambda) = \frac{A_{SW}(\lambda) \times \ln 10}{\ell} \qquad \text{(A.6)}$$

Transmission spectra of the glass incubation vessels ($T(\lambda)$; Fig. A1) were recorded using the same instrument on which the liposome and seawater absorbance spectra were acquired; these $T(\lambda)$ were recorded as fractions.

A.3.2. Results

The capacity of PC 22:6, 22:6 to absorb light in both the UVB and UVA spectral bands exceeded by more than an order of magnitude those of direct molecular analogs containing fully saturated (PC 22:0, 22:0) and monounsaturated (PC 22:1, 22:1) fatty acids of the same chain length (Fig. A4c); the large difference we observed between the molar absorptivity of the hexa-unsaturated compound and its more saturated analogs was corroborated by similar results previously reported for other sequences of related phospholipids (McHowat et al., 1996; Spector et al., 1996). In addition, UV-visible absorbance measurements of docosahexaenoic acid, the constituent fatty acid of PC 22:6, 22:6, indicated that the parent molecule's light-absorbing capacity was due primarily to the presence of the highly unsaturated acyl moiety and not the polar headgroup (Fig. A4b,c). Absorbance measurements of the lipid standards were repeated for verification in three independent experiments over the course of two months. While no molar absorptivity data have been published for PC 22:6, 22:6 or other individual IP-DAG, the $\varepsilon_i(\lambda)$ we calculated for DHA agreed generally with values found in the literature (Whitcutt, 1957).

A.4. Collection of water column lipid samples

A.4.1. Methodological details

In addition to the photooxidation experiments, water samples were collected in 2013-2014 for lipid analysis from Arthur Harbor (at LTER Station B; Fig. 1b) and at stations offshore (PAL-LTER cruise LMG1401 aboard the ARSV *Laurence M. Gould*). Persistent sea ice in the immediate vicinity of Palmer Station prevented regular collection of samples there until mid-December 2013; samples from the *Gould* cruise were collected in January 2014 at distances of 50-300 km from shore.

A.5. Mass spectrometer settings and analysis of HPLC-ESI-MS data

A.5.1. Sample injection, chromatography and ESI source settings

For both the water column samples and those from the liposome experiments, 20 μL injections of sample extract were made onto a C8 Xbridge HPLC column (particle size 5 μm, length 150 mm, width 2.1 mm; Waters Corp., Milford, MA, USA). Eluent A consisted of water with 1% 1M ammonium acetate and 0.1% acetic acid. Eluent B consisted of 70% acetonitrile, 30% isopropanol with 1% 1M ammonium acetate and 0.1% acetic acid. Gradient elution was performed with the following program (total run time 40 min) at a constant flow rate of 0.4 mL min^{-1}: 45% A for 1 min to 35% A at 4 min, then from 25% A to 11% A at 12 min, then to 1% A at 15 min with an isocratic hold until 30 min, and finally back to 45% A for 10 min column equilibration. ESI source settings were: Spray voltage, 4.5kV (+), 3.5 kV (-); capillary temperature, 200°C; sheath gas and auxiliary gas, both 20 (arbitrary units); heated ESI probe temperature, 350°C. All chemicals used in sample extraction and chromatography were LC/MS grade or higher. Where used, water was obtained from a Milli-Q system without further treatment (EMD Millipore, Billerica, MA, USA).

A.5.2. Mass spectrometer acquisition settings

Mass data were collected on a Thermo Q Exactive Hybrid Quadrupole-Orbitrap mass spectrometer (ThermoFisher Scientific, Waltham, MA, USA) instrument in full scan and TopN data dependent-MS^2 (dd-MS^2) acquisition modes while alternating between positive and negative ionization modes. Following the full spectrum scan in each mode (scan range of 100-1500 *m/z*), the five ions of highest intensity were selected using the quadrupole for MS^2 fragmentation. Data were acquired in the following sequence: FT positive full lock MS, positive-mode dd-MS^2, FT negative full lock MS, and negative-mode dd-MS^2. The S-lens RF level and voltage were set to 100.00% and 25.00 V, respectively. Mass resolution was set to the maximum possible value of 140,000 (FWHM at *m/z* 200) for full scan acquisition and to 17,500 for dd-MS^2 scans. The full scan mass resolution setting corresponded to an observed resolution of 75,100 at the *m/z* (875.5505) of our internal standard, DNP-PE, in positive ion mode. Using these settings, we obtained between 8 and 14 MS scans across a typical peak in full scan mode. The following other settings were applied: MS^2 isolation window, 4 *m/z*; MS^2 isolation offset, 0.00; loop count, 5; dynamic exclusion, 10.0 s; AGC target, 3,000,000/100,000 (full scan/MS^2); skimmer voltage, 15.00 V; inject flatapole DC, 6.00; MP2 and MP3 RF, 594; gate lens voltage, 5.88 V; C-trap RF, 1,010; MS^2 NCE/stepped NCE, 30, 50, 80.

A.5.3. Procedures used for weekly and real-time calibration of the Exactive

The mass spectrometer was calibrated as required in both positive and negative ion modes by infusing calibration mixes available from ThermoFisher Scientific. Deliberate lock masses were also used for real-time recalibration; $C_{16:0}$ (*m/z* 255.23295) and $C_{18:0}$ (*m/z* 283.26425) fatty acids were used in negative ion mode, while ammonium adducts of a series of polysiloxanes (*m/z* 536.16537, 610.1842, and

684.2035) were used in positive ion mode. At least one of the lock masses was found during each positive and negative full scan event.

A.5.4. Identification and quantification of lipids & oxidized lipids

All HPLC-ESI-MS data were analyzed in R (R Core Team, 2016) using open-source tools according to the lipidomics workflow described in Collins et al. (2016). MS data were first converted from vendor format using msConvert (Kessner et al., 2008); xcms (Benton et al., 2010; Smith et al., 2006; Tautenhahn et al., 2008) and CAMERA (Kuhl et al., 2012) were then used for peak-picking, retention time alignment, and identification of secondary isotope peaks. The LOBSTAHS lipidomics discovery software (Collins et al., 2016) was used to putatively identify the processed, high-quality MS features based on exact mass, retention time, and diagnostic adduct hierarchy. For intact PC species and their constituent fatty acids in the liposome experiment data, we confirmed each putative identification from the LOBSTAHS software using two additional means: (1) via comparison of data-dependent MS^2 spectra with those from authentic standards or published reference spectra and (2) by requiring the presence of the same compound identity in data acquired in the opposite HPLC-ESI-MS ionization mode. These orthogonal criteria allowed us to identify the various intact PC species with a high level of confidence falling somewhere between levels 1 and 2 in the proposed scheme of Sumner et al. (2007) for metabolite identification. We confirmed the basic identities of lysophosphatidylcholine (LPC) and oxidized PC (ox-PC) species based on the presence of four or more diagnostic PC headgroup fragments in the relevant MS^2 spectrum.

We were unable to definitively identify the structures of these oxidized and lyso species in all cases because (1) our MS method did not yield fragmentation spectra at levels > MS^2 and (2) commercial standards do not exist for the vast majority of ox-PC species. However, using exact mass, headgroup fragments, and retention time, we identified nearly all of these compounds with a confidence falling somewhere between levels 2 and 3 in the Sumner et al. (2007) scheme. Finally, for the water column lipid data, we required the presence of each putatively identified compound in both HPLC-ESI-MS ionization modes. In these instances, we confirmed all LOBSTAHS identities using a new, experimental LOBSTAHS feature which automatically detects diagnostic product ion fragments and constant neutral losses for each lipid class (as given in Popendorf et al., 2013) in the available data-dependent MS^2 spectra for each sample. For the compounds identified in the environmental (water column) data, we thus achieved a confidence approaching level 2 in the Sumner et al. (2007) scheme.

For quantification of IP-DAG, authentic standards were obtained either from natural extracts or from the same source (Avanti Polar Lipids) as the lipids used in the liposomes (Popendorf et al., 2013; Van Mooy and Fredricks, 2010). For quantification of docosahexaenoic acid (DHA), an authentic

standard was obtained from Nu-Chek Prep Inc. (Elysian, MN, USA). For LPC and ox-PC species, we applied the standard curve for the corresponding intact, unoxidized molecule; authentic standards are commercially available for only a small fraction of the many possible intact ox-PC species and their isomers. The concentration of each analyte was then normalized to the concentration in the same sample of the internal standard, DNP-PE. 20 μL of DNP-PE was added to all particulate lipid samples during the first step of the modified Bligh and Dyer extraction; for the liposome experiments, we added 30 μL of DNP-PE to the separatory funnel prior to performing the liquid/liquid extraction.

A.6. Determination of apparent quantum yield (AQY)

A.6.1. Calculation of additional terms in Eq. 2

We calculated $\alpha_{tot}(\lambda)$ in Eq. 2 as the sum of the Napierian absorption coefficient of the filtered seawater matrix and the Napierian absorptivities of the lipids present in the vial at the time of the experiment, i.e.,

$$\alpha_{tot}(\lambda) = \alpha_{SW}(\lambda) + \kappa_i(\lambda)C_i + \kappa_j(\lambda)C_j + \ldots + \kappa_n(\lambda)C_n \qquad \text{(A.7)}$$

where $\kappa_i(\lambda)$ and $\kappa_j(\lambda) \ldots \kappa_n(\lambda)$ are the wavelength-specific molar Napierian absorption coefficients of lipid *i* and the other lipid species evaluated in each experiment, respectively (Fig. A4; the species evaluated in each experiment are given in Table A1). $F_i(\lambda)$ in Eq. 2 was calculated after Miller (1998) as the ratio of the Napierian absorptivity of lipid *i* to the total absorptivity:

$$F_i(\lambda) = \frac{\kappa_i(\lambda)C_i}{\alpha_{tot}(\lambda)} \qquad \text{(A.8)}$$

A.6.2. Monte Carlo method for determination of uncertainty in AQY

First, where possible, we determined uncertainties for all individual parameters in Eqs. 2, A.7, and A.8 from experimental replication or, in the case of data obtained from single samples using the benchtop spectrophotometer, repeated analytical measurements. We then conducted a series of 10,000 simulations in which a new value for each parameter was chosen at random from a normal distribution constructed from the parameter's mean value and analytical or observational uncertainty as its standard deviation. (In the case of z_{eff}, to which we assigned an additional uncertainty of + 100 %, we used a half-normal distribution such that 1.8 cm was always the minimum possible value chosen.) In each simulation, the randomly chosen values from these distributions were used to obtain a different estimate of the AQY from Eqs. 2, A.7, and A.8; the uncertainties in our estimates of $K_d(\lambda)$ (Fig. A3) were included in analysis. The final uncertainty in each AQY estimate was determined from the set of 10,000 estimates generated during the simulation using the method of Desharnais et al. (2015) for bootstrap estimation of confidence intervals in non-normal data. We expected that the asymmetrical uncertainty associated with the z_{eff} term would introduce some skewness into the distribution of estimates generated during the

Monte Carlo simulation, precluding the use of the standard deviation of the set of simulation estimates as a simple estimator of the final uncertainty. The R code we used to conduct the simulation is available online; a link is provided below. Although we assumed normal distributions for each parameter in the simulations other than z_{eff}, we could not be absolutely certain the underlying populations were normally distributed because of the small sample sizes.

A.6.3. Additional possible bias in method used to estimate AQY

The use of Eq. 2 to calculate an AQY requires that samples be optically thin (i.e., that $\alpha_{tot} \times z_{eff} \ll 1$; (Hu et al., 2002). This condition appeared to be satisfied: The maximum $\alpha_{tot}(\lambda)$ we recorded in any of the liposome solutions was 0.17 m^{-1} at 304 nm. Assuming a pathlength of 4 cm, this equated to an absorbance of 6.8×10^{-4}.

A.7. Lipid photooxidation rate estimates for natural waters of West Antarctica

Photooxidation rates were calculated according to the equation

$$\frac{-d[lipid]}{dt} = \Phi_{UVR} \int_{290}^{395.5} \frac{E_{n,\mathrm{p},\Sigma}(\lambda)\left(1-e^{-K_d(\lambda)z}\right)}{z} F_{lipid}(\lambda) d\lambda \qquad \text{(A.9)}$$

where $[lipid]$ is the measured concentration (in pmol L^{-1}) of lipids in the respective saturation fraction; Φ_{UVR} is the broadband AQY determined as described above; $K_d(\lambda)$ is the appropriate Napierian downwelling attenuation coefficient for Arthur Harbor calculated in Eq. A.1; $E_{n,\mathrm{p},\Sigma}(\lambda)$ is the daily downwelling photon flux (μmol photons m^{-2} d^{-1}) estimated at depth z (from application of the appropriate $K_d(\lambda)$ to the incident SUV-100 time-series data, as described in Section A.2.1); and $F_{lipid}(\lambda)$ is the ratio of the Napierian absorptivity of lipids in the indicated fraction to the total absorptivity.

We approximated $F_{lipid}(\lambda)$ in Eq. A.9 as

$$F_{lipid}(\lambda) = \frac{\kappa_i(\lambda) C_{lipid}}{K_d(\lambda)} \qquad \text{(A.10)}$$

where $\kappa_i(\lambda)$ is the molar Napierian absorption coefficient for the unsaturated compound, PC 22:6, 22:6, at wavelength λ and C_{lipid} is the measured concentration (in pmol L^{-1}) of lipids in the respective saturation fraction, equivalent to $[lipid]$ above. We applied the measured $\kappa_i(\lambda)$ for PC 22:6, 22:6 to all lipids containing multiple polyunsaturated fatty acids based on our observations of the effect of polyunsaturation on specific absorbance in IP-DAG (Fig. A4) and previous evidence (see Section 4.1 in main text); in addition, it would have been highly impractical within the scope of the present work to measure specific $\kappa_i(\lambda)$ for the hundreds of different IP-DAG we observed in the natural samples. Using Eq. A.9, we calculated rates of lipid photooxidation at 1 m intervals from the ocean's surface to the depth of the mixed layer; these volumetric rate estimates were integrated to yield areal estimates of the lipid

photooxidation rate for each day during the study period (units of pmol lipid m^{-2} d^{-1} or pmol C m^{-2} d^{-1}; mixed layer depth data, Table A2). Uncertainities in lipid photooxidation rates calculated from Eq. A.9 were estimated using the same Monte Carlo approach described in Section A.6.2.

A.8. Conversion factors

A.8.1. Conversion factors for bacterial production rates

For the PAL-LTER bacterial production data, rates of leucine incorporation in pmol L^{-1} hr^{-1} were converted to units of mg C m^{-3} d^{-1} assuming a conversion factor of 1.5 kg C (mol leucine)$^{-1}$ and isotope dilution of 1, after making the necessary adjustments for time and volume.

A.8.2. Conversion factors applied to photooxidation rate estimates, and associated assumptions

We converted the photooxidation rate estimates presented in Section 4.2 and Fig. 9 from units of lipid (i.e., pmol IP-DAG L^{-3} d^{-1}) to carbon based on the carbon content of the IP-DAG identified in each unsaturation fraction; these were 49. 3 ± 0.5 and 50.6 ± 0.6 mol C : mol lipid for the polyunsaturated (cyan) and highly polyunsaturated (red) fractions, respectively. In our calculations, we assumed that the vast majority of initial oxidation products — such as the ox-PC we identified in the HPLC-ESI-MS data — would further degrade into smaller molecular components, while initiating the degradation of other nearby lipids (and other molecules) that contain easily abstracted hydrogen atoms (Crastes de Paulet et al., 1988). However, we acknowledge here the many adaptations to oxidative stress possessed by phytoplankton, including considerable capacity to dissipate ROS and dozens of mechanisms for repair of damage to oxidized biomolecules (Roy, 2000). It is thus possible, as Rontani et al. (2016) have suggested based on observations in the Arctic, that the lipids in living phytoplankton cells may be much less susceptible to photooxidation than lipids in senescent or dead biomass. We note that in the 2016 study, Rontani et al. did not look for evidence of photooxidation in intact lipids (i.e., ox-IPL) or in the oxidized products of lipids containing fatty acids with more than one double bond.

A.9. Availability of data and code

All final, original data presented in this work, including lipid data from the diatom cultures and water column samples, have been archived to PANGAEA at https://doi.org/10.1594/PANGAEA.879582 and may be cited by DOI. All R scripts and R data objects required to reproduce the results and figures in this work are available online and may be cited by DOI at https://doi.org/10.5281/zenodo.841929; individual files may be downloaded directly at https://github.com/jamesrco/LipidPhotoOxBox. All PAL-LTER data used in this manuscript were downloaded from the Palmer LTER Datazoo at http://oceaninformatics.ucsd.edu/datazoo/data/pallter/datasets and the NOAA spectroradiometer data

were downloaded from http://www.esrl.noaa.gov/gmd/grad/antuvdata/. Raw MS data files (> 200 MB) and raw spectral data collected using the Jaz instrument are available upon request from the author.

Supplementary figures

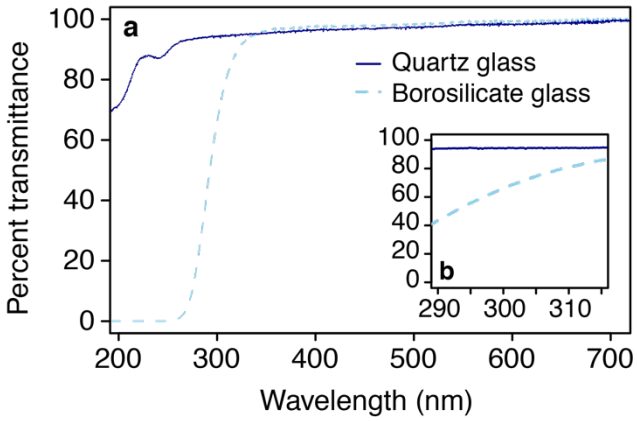

Fig. A1. (a) Transmission spectra ($T(\lambda)$) of the glass incubation vessels used in lipid photooxidation experiments measured with a dual-path benchtop spectrophotometer. (b) Inset, showing transmissivities in the UVB spectral band (290-315 nm).

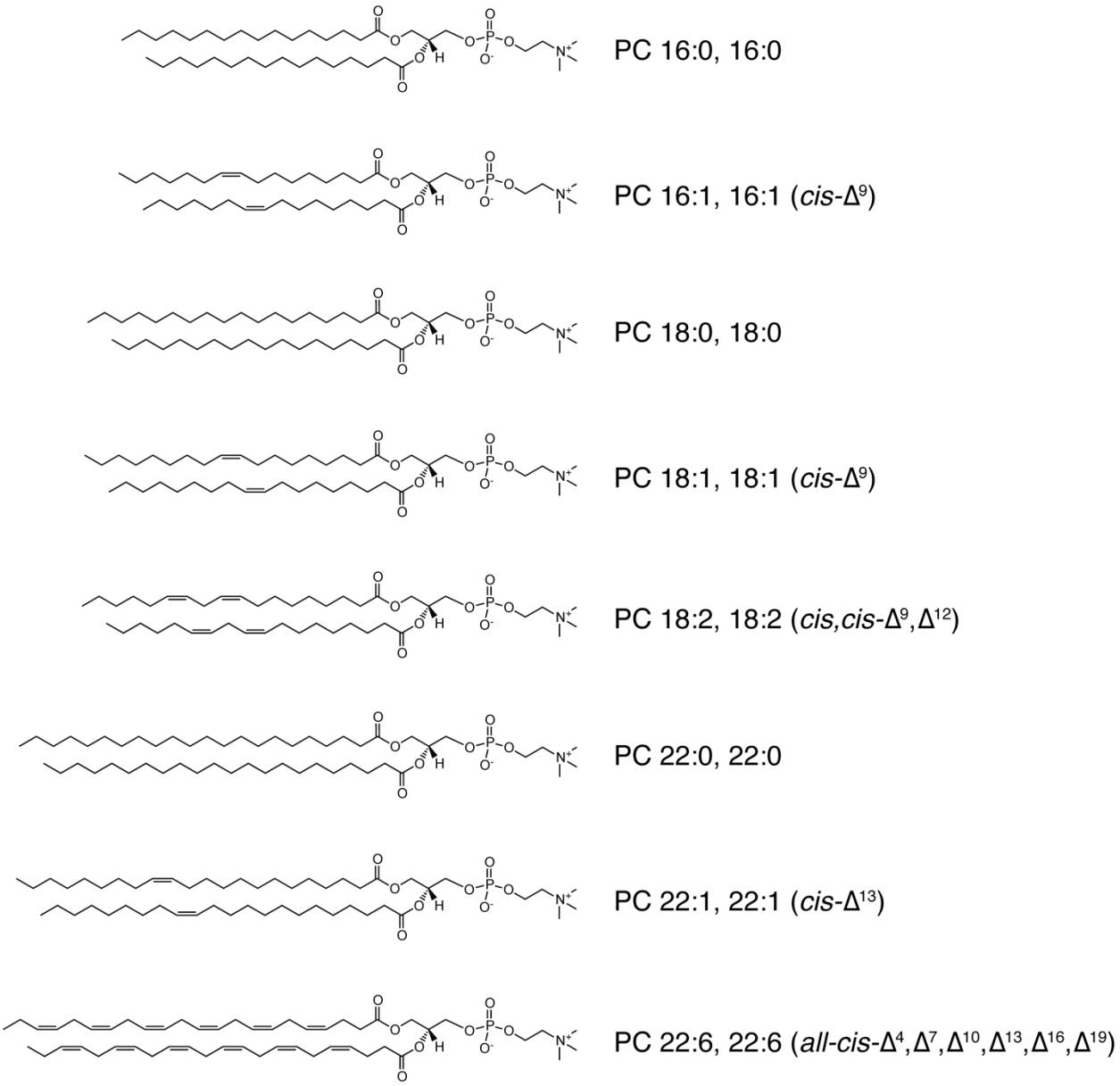

Fig. A2. Structures of the eight species of phosphatidylcholine (PC) evaluated in the photooxidation experiments.

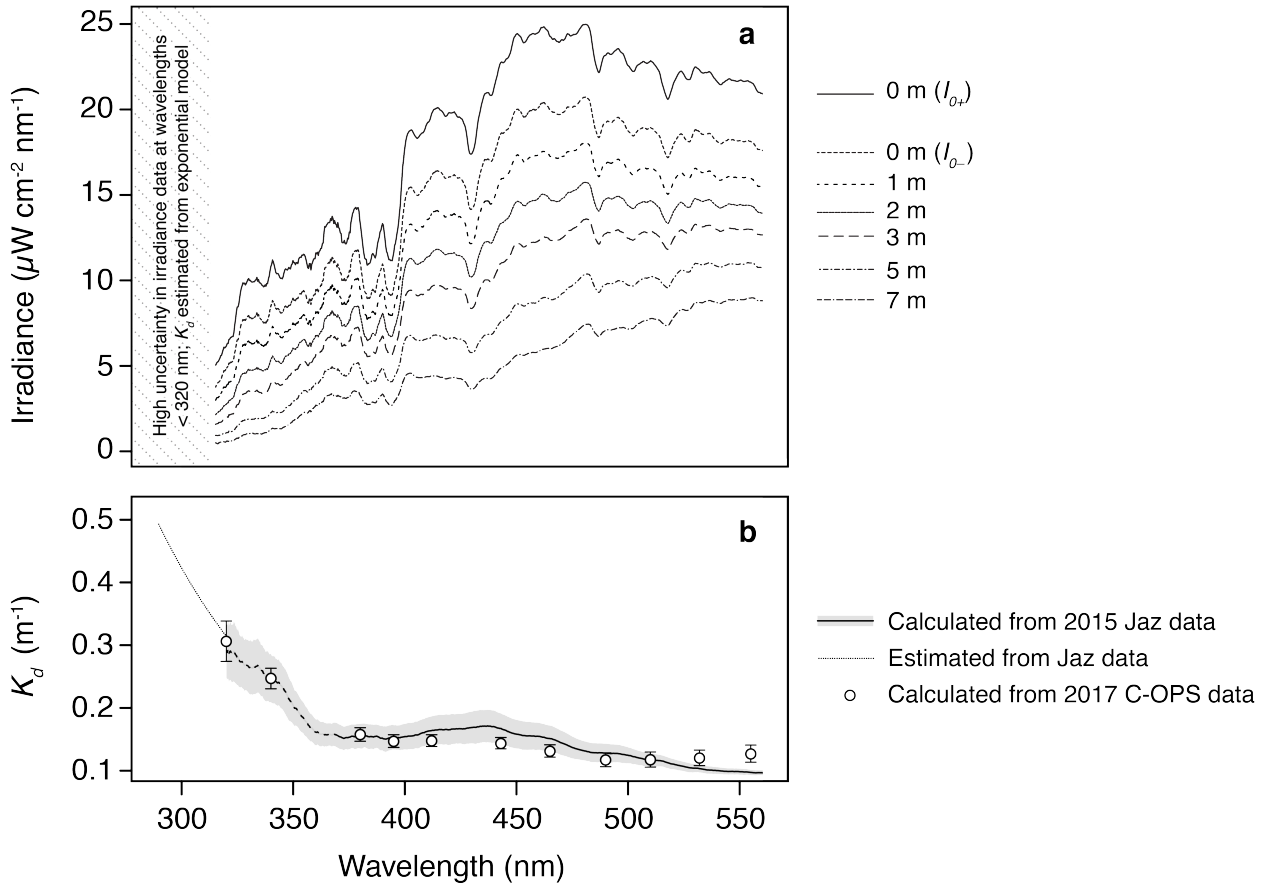

Fig. A3. (a) Wavelength-specific measurements of downwelling irradiance at 7 depths in Arthur Harbor (PAL-LTER Station B) made with the Jaz spectrophotometer on 15 December 2015. (b) $K_d(\lambda)$ for the same waters, calculated using the data in (a). $K_d(\lambda)$ for 320-550 nm (dashed and solid black trace; mean of n = 14 observations at each wavelength) were calculated directly from the depth profile data according to Eq. A.1. Area of shading indicates uncertainty (mean ± standard deviation). $K_d(\lambda)$ for 290-320 nm (dotted trace) were estimated using an exponential model ($K_d = e^{-0.0149\lambda+3.60}$) fit to the data from the 320-370 nm interval (dashed section). Superimposed are independent estimates of $K_d(\lambda)$ calculated from data collected with a C-OPS profiling instrument (Biospherical) at the same location on 16 November 2017 (mean ± standard deviation of n = 1,052 observations at each wavelength). Acquisition and analysis of the C-OPS data are described in Section A.2.2. All $K_d(\lambda)$ were calculated in Napierian mode. The Jaz-derived $K_d(\lambda)$ for wavelengths 290-700 nm are given in Table A3.

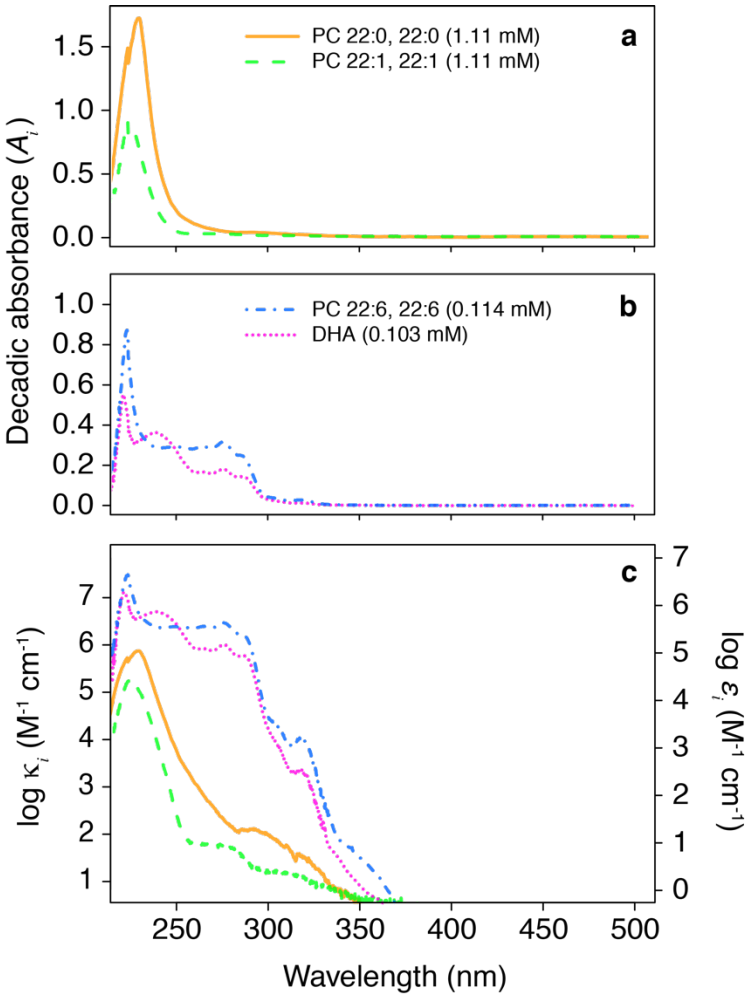

Fig. A4. Effect of acyl unsaturation on photochemical potential in the membrane lipid phosphatidylcholine (PC) and constituent fatty acid docosahexaenoic acid (DHA). (a) Wavelength-specific decadic absorbances ($A_i(\lambda)$) of equimolar (1.11 mM) concentrations of PC 22:0, 22:0 and PC 22:1, 22:1 (*cis*-Δ^{13}) dissolved in methanol. (b) Wavelength-specific decadic absorbances of PC 22:6, 22:6 (*all-cis*-Δ^4,Δ^7,Δ^{10},Δ^{13},Δ^{16},Δ^{19}) and DHA at concentrations in methanol of 0.114 and 0.103 mM, respectively. (c) Molar absorption coefficients for the four species in Napierian (κ_i) and decadic (ε_i) units, calculated according to Eq. A.5.

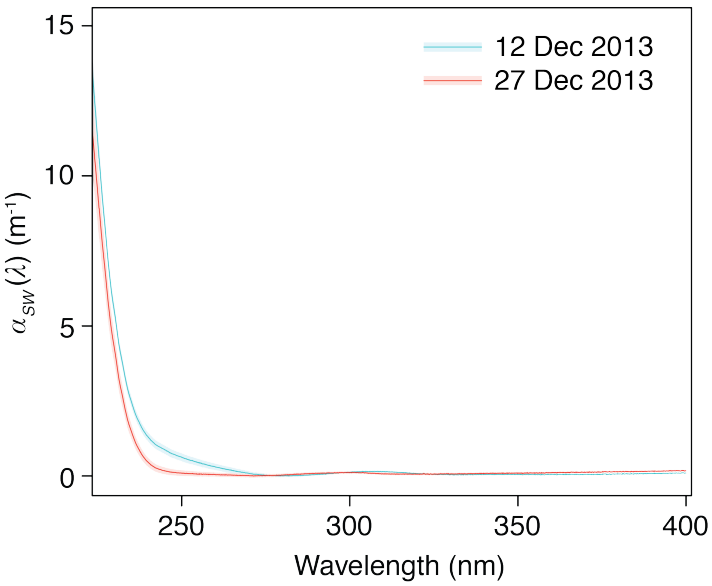

Fig. A5. Wavelength-specific linear Napierian absorption coefficients ($\alpha_{SW}(\lambda)$) of West Antarctic Peninsula surface waters from samples collected on two dates in December 2013. For each date, we report the mean values of $\alpha_{SW}(\lambda)$ determined for each wavelength in a set of samples collected at 0, 5, and 10 m. The 27 December values (red trace) reflect samples collected at the three depths at both PAL-LTER time series stations (B and E; n = 6), while the 12 December values (blue trace) are based only on samples collected at Station B (n = 3). The shaded region surrounding each trace depicts one standard deviation. Values of $\alpha_{SW}(\lambda)$ were calculated according to Eq. A.6.

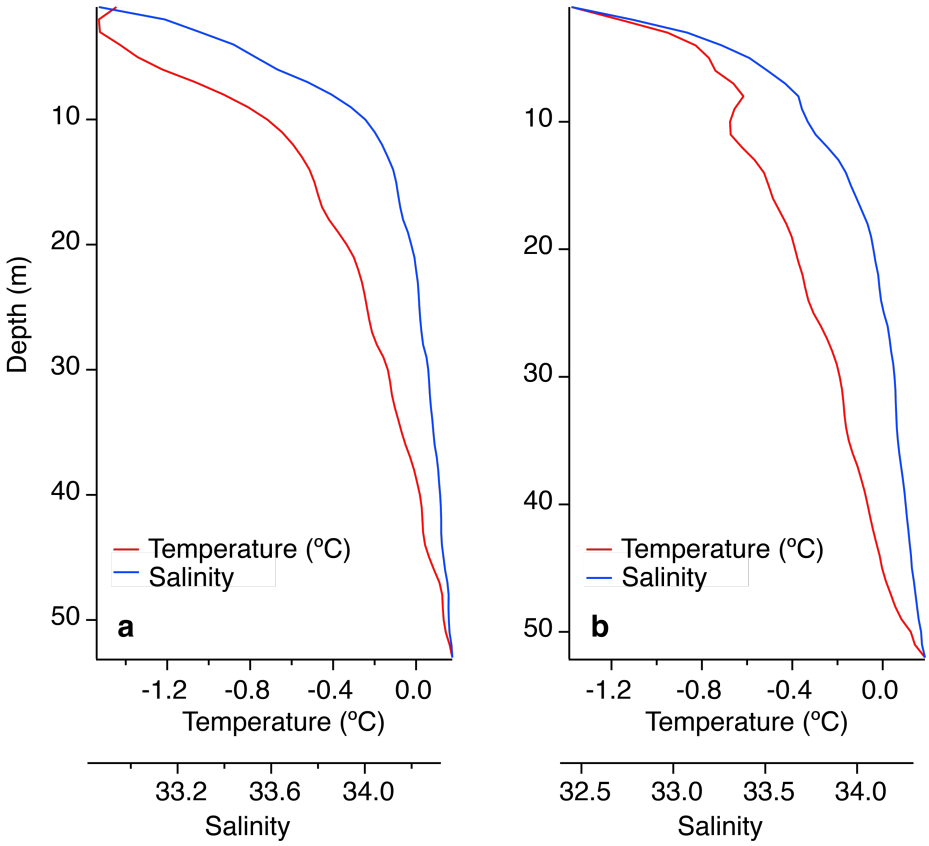

Fig. A6. Profiles of temperature and salinity made at PAL-LTER Station B on (a) 12 December and (b) 24 December 2013. The mixed layer depth was between 7-8 m on 12 December and 5 m on 24 December. The MLD was defined according to Levitus (1982) as the depth at which the temperature difference from the surface was 0.5°C. The data from which these figures were constructed were retrieved from http://oceaninformatics.ucsd.edu/datazoo/data/pallter/datasets?action=summary&id=228 on 1 November 2016; additional mixed layer depth estimates are presented in Table A2. The location of Station B in Arthur Harbor is shown in Fig. 1.

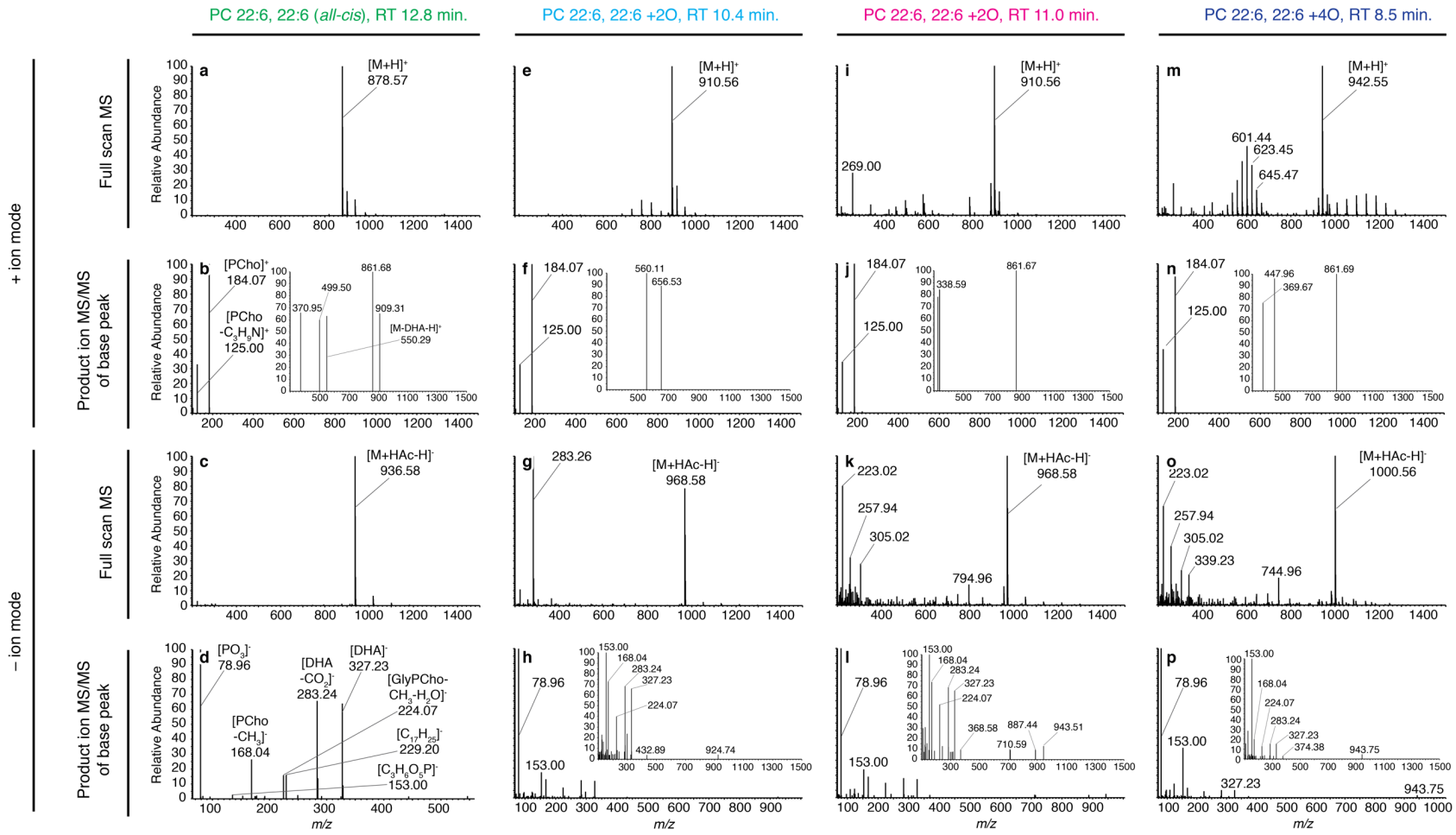

Fig. A7. Expanded version of Fig. 6 in the main text, showing annotated positive and negative ion mode spectra used to identify three intact oxidized products of PC 22:6, 22:6 (*all-cis*-Δ^4,Δ^7,Δ^{10},Δ^{13},Δ^{16},Δ^{19}) in a lipid photooxidation experiment on 14 December 2013. The spectra presented here are from one of three replicate samples of the + UVR - het. bact. treatment at the final experimental time point shown in Fig. 4. Product ion spectra (second and fourth rows) were obtained via data-dependent MS^2 using a Thermo Q Exactive Hybrid Quadrupole-Orbitrap mass spectrometer; MS and HPLC conditions are described in Section A.5. Panels (a)-(d) show diagnostic spectra for the intact parent PC 22:6, 22:6 molecule ($[M+H]^+$ and $[M\text{-}HAc\text{-}H]^-$ adducts, respectively); these were validated by comparison with an authentic standard. Panels (e)-(h), (i)-(l), and (m)-(p) show, respectively, spectra for three ox-PC 22:6. 22:6 species identified at 10.4, 11.0, and 8.5 min. Colors in column headings

correspond to those used in Fig. 5 and Fig. 6 in the main text. Insets show the relative intensities of ions ≥ 300 or 100 *m/z* units (positive and negative ionization modes, respectively). Although we were unable to identify the precise structures of the three ox-PC species without further fragmentation (i.e., MS^n; see discussion in main text), we offer five lines of evidence for identities of these species as +2O and +4O products of the parent molecule, with the additional conviction that the oxidation in each case occurred at a specific position on one of the two attached acyl chains: (1) the knowledge that, by virtue of the experimental design, the observed species must be degradation products of one of the five lipids we added as liposomes, (2) agreement at ≤ 0.3 ppm of the exact masses of the parent ion adducts in both ionization modes with calculated theoretical masses, (3) systematic shifts in retention time consistent with the progressive addition of oxygen atoms, (4) the unique fragmentation spectra observed, each containing ions not present in those obtained for the parent molecule, and (5) the presence in all three of the negative ion mode MS^2 spectra of the *m/z* 327.23, 224.07, and 283.24 fragments diagnostic of the presence of intact, unoxidized DHA.

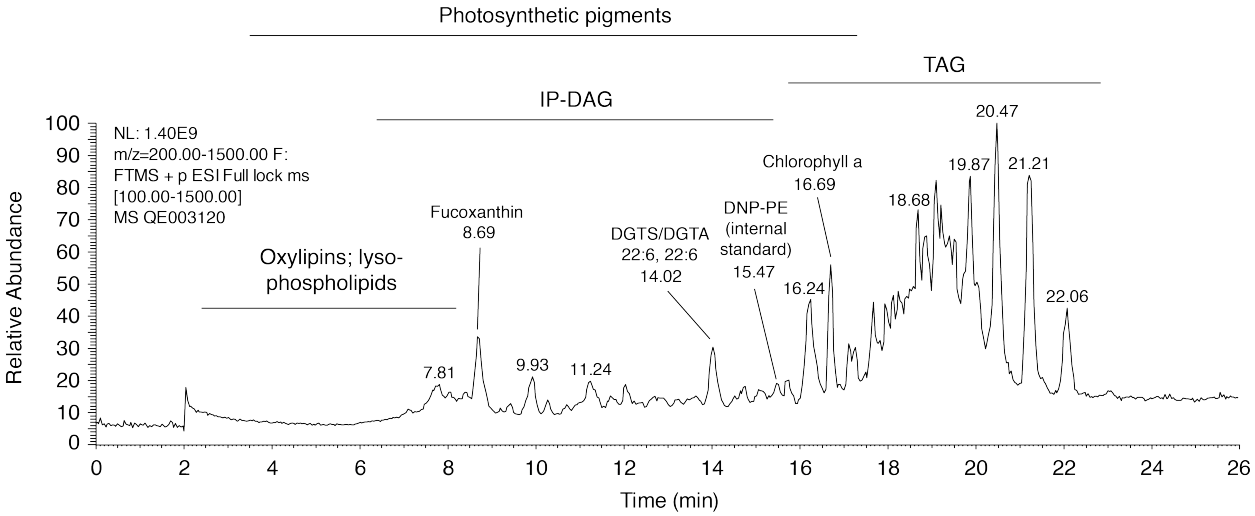

Fig. A8. Total ion current chromatogram (all features, *m/z* 200-1500, positive ionization mode) of a particulate marine lipid sample from the West Antarctic Peninsula. Annotations show major features and retention time ranges for various classes of lipid. This figure shows the same water column sample from Station E, Arthur Harbor, West Antarctica, which is presented in the leftmost position in Fig. 7 and Fig. 8, and which is described in Table A5. HPLC-ESI-MS analysis and subsequent identification and screening of lipids were performed as described in the main text.

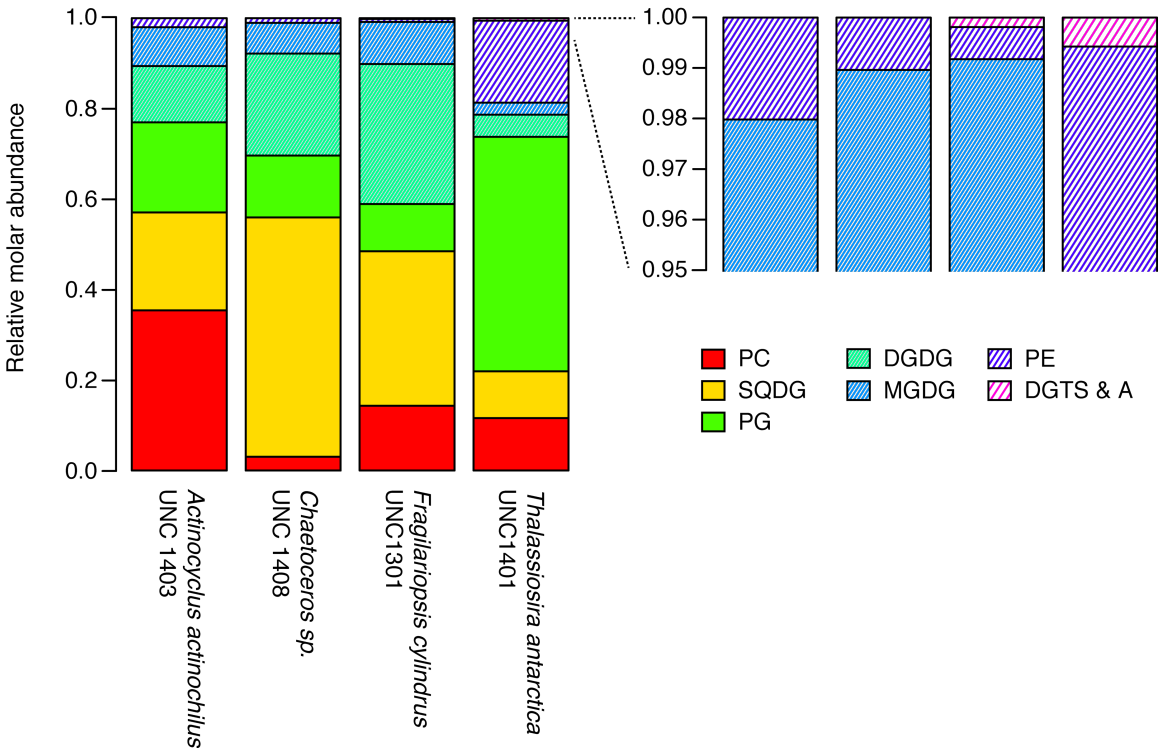

Fig. A9. Relative molar distribution of seven classes of intact polar diacylglycerol (IP-DAG) in cultures of four diatoms isolated from waters of the West Antarctic Peninsula. Cultures were grown in nutrient replete medium and biomass was harvested in exponential growth phase. Lipids were identified using the LOBSTAHS software and several additional criteria described in the main text; the data in this figure represent 316 different IP-DAG identified in the four isolates. Quantification of lipids was performed using authentic standards as described in the main text. We also identified several species of diacylglyceryl carboxyhydroxymethylcholine (DGCC) in the isolates; these were excluded from the dataset used to generate the figure because we did not have a suitable authentic standard available at the time of analysis. DGCC accounted for < 1 % of the total raw IP-DAG peak area in *A. actinochilus* and *F. cylindrus*, < 3 % in *Chaetoceros sp.*, and ~ 20 % of the total IP-DAG peak area in *T. antarctica*. The diatom cultures were kindly provided by C. Moreno and A. Marchetti, University of North Carolina. The full, annotated list of the lipids identified in each culture is available online at https://github.com/jamesrco/LipidPhotoOxBox/blob/master/data/nice/LOBSTAHS_lipid_identities/UNC_Marchetti_diatom_cultures_IP-DAG_pmol_totals.final.csv or https://doi.org/10.1594/PANGAEA.879582.

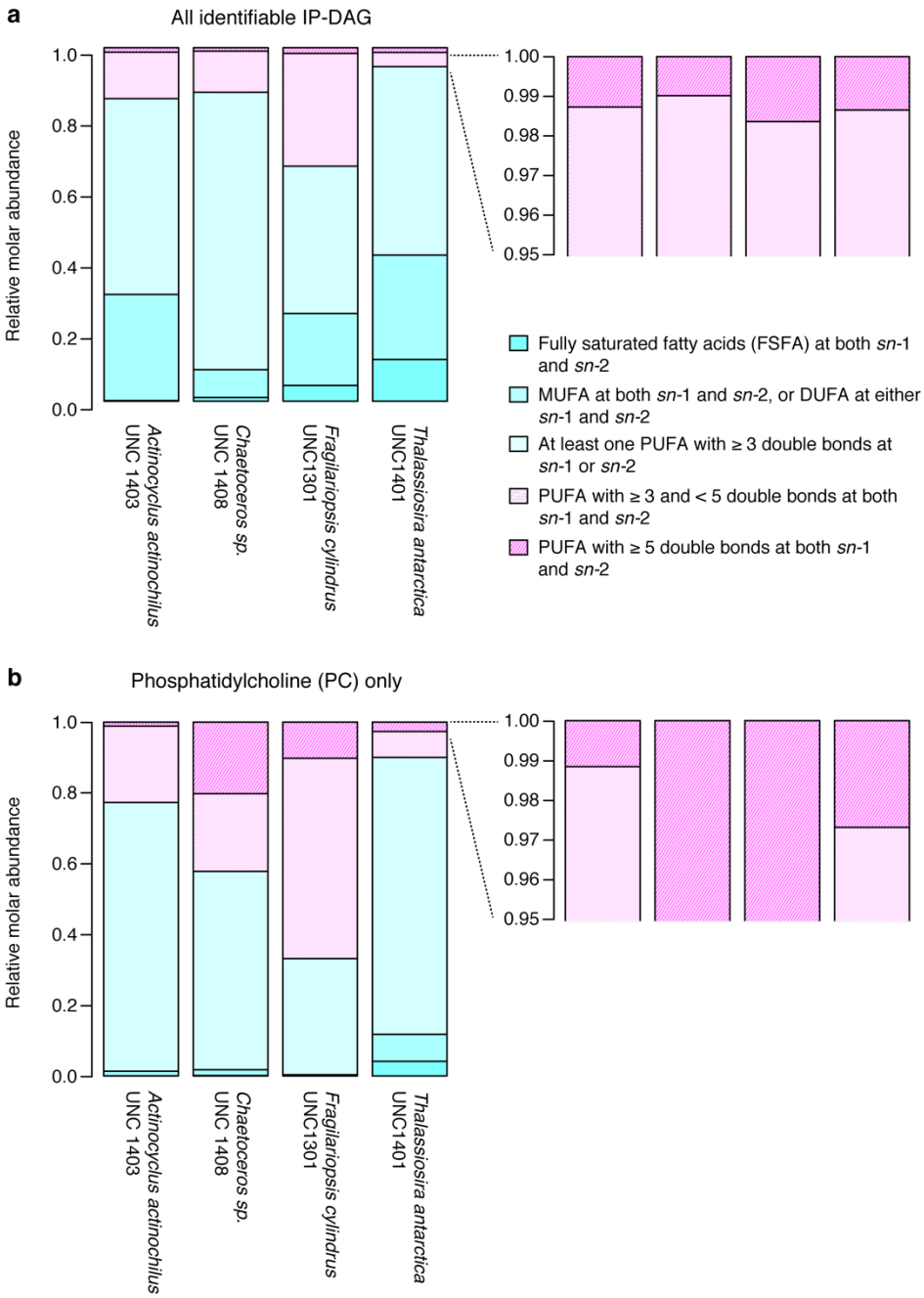

Fig. A10. Fatty acid composition of (a) all identifiable IP-DAG and (b) phosphatidylcholine (PC) species in the four Antarctic diatom isolates for which distributions of IP-DAG are presented in Fig. A9. Because the current version of the LOBSTAHS software resolves the identities of IP-DAG only to the level of bulk fatty acid composition (i.e., the sum of the properties of the substituents at both the *sn*-1 and *sn*-2 positions), we were unable to determine which fatty acids were present in each molecule without additional inspection of fragmentation spectra or saponification for analysis fatty acid methyl esters (FAMES). We were able to categorize the saturation state of the IP-DAG according to the simplified scheme we present here after verifying (by inspection of fragmentation spectra) that the maximum degree of unsaturation of any single fatty acid present in these species was six (present in the form of docosahexaenoic acid, or DHA).

Table A1
Summary of results from liposome photooxidation experiments.

Moiety phosphatidyl-choline	No. independent experiments in which evaluated	Date of experiment (2013)	Change in concentration[a] (pmol mL^{-1} ± SE)				
			Treatment				
			Control (dark) - het. bact.	Control (dark) + het. bact	+ UVR (quartz vial) - het. bact.[b]	+ UVR (quartz vial) + het. bact.[c]	Boro-silicate vial - het. bact.[d]
PC 16:0/16:0	5	9 Oct	ns[e]	–[f]	ns	–	ns
		30 Oct	ns	–	ns	–	ns
		20 Nov	ns	ns	ns	ns	ns
		2 Dec	ns	–	ns	–	ns
		14 Dec	ns	ns	ns	ns	ns
PC 16:1/16:1	3	9 Oct	ns	–	ns	–	ns
		30 Oct	ns	–	ns	–	ns
		20 Nov	ns	ns	ns	ns	ns
PC 18:0/18:0	5	9 Oct	ns	–	ns	–	ns
		30 Oct	ns	–	ns	–	ns
		20 Nov	ns	ns	ns	ns	ns
		2 Dec	ns	–	ns	–	ns
		14 Dec	ns	ns	ns	ns	ns
PC 18:1/18:1	4	9 Oct	ns	–	ns	–	ns
		30 Oct	ns	–	ns	–	ns
		20 Nov	ns	ns	ns	ns	ns
		14 Dec	ns	ns	ns	ns	ns
PC 18:2/18:2	2	9 Oct	ns	–	ns	–	ns
		20 Nov	ns	ns	ns	ns	ns
PC 22:0/22:0	2	2 Dec	ns	–	ns	–	ns
		14 Dec	ns	ns	ns	ns	ns
PC 22:6/22:6	2	2 Dec	ns	–	ns	–	ns
		14 Dec	-322 ± 229	-223 ± 307	**-804 ± 188***	**-827 ± 190***	**-634 ± 182**

[a] Reported only where mean final concentration in at least one treatment was significantly different from mean initial concentration according to Tukey's "Honest Significant Difference" method with $\alpha = 0.05$: $p \leq 0.05$ (**bold**), $p \leq 0.01$ (*); rates are reported as mean ± SE of n ≥ 3 replicates.
[b] Quartz glass vessel; 0.2 µm filtered seawater
[c] Quartz glass vessel; 0.7 µm filtered seawater
[d] Borosilicate glass vessel; 0.2 µm filtered seawater
[e] ns: not significant
[f] Treatment combination was not evaluated in this experiment

Table A2
Mixed layer depths in December 2013 and January 2014, Arthur Harbor, West Antarctica.

Date	Station[a]	Estimated depth of mixed layer (m)[b]
12 Dec 2013	B	7
24 Dec 2013	B	5
27 Dec 2013	B	10
	E	15
2 Jan 2014	B	22
	E	19

[a] Stations occupied by the PAL-LTER study in Arthur Harbor; see Fig. 1.
[b] The mixed layer depth was defined according to Levitus (1982) as the depth at which the temperature difference from the surface was 0.5°C; full profiles of temperature and salinity measured at Station B on 12 and 24 December are presented in Fig. A6.

Table A3
Napierian downwelling attenuation coefficients ($K_d(\lambda)$) for West Antarctic mixed layer waters

λ	$K_d(\lambda)$	λ	$K_d(\lambda)$	λ	$K_d(\lambda)$	λ	$K_d(\lambda)$
289.7	*0.49*[a]	306.0	*0.39*	322.3	0.30	338.5	0.25
290.1	*0.49*	306.4	*0.38*	322.7	0.30	338.8	0.25
290.5	*0.49*	306.8	*0.38*	323.0	0.30	339.2	0.25
290.8	*0.48*	307.1	*0.38*	323.4	0.30	339.6	0.25
291.2	*0.48*	307.5	*0.38*	323.8	0.30	340.0	0.25
291.6	*0.48*	307.9	*0.38*	324.1	0.30	340.3	0.25
292.0	*0.48*	308.3	*0.37*	324.5	0.29	340.7	0.24
292.3	*0.47*	308.6	*0.37*	324.9	0.29	341.1	0.24
292.7	*0.47*	309.0	*0.37*	325.2	0.29	341.4	0.24
293.1	*0.47*	309.4	*0.37*	325.6	0.29	341.8	0.24
293.4	*0.47*	309.7	*0.37*	326.0	0.29	342.2	0.24
293.8	*0.46*	310.1	*0.36*	326.3	0.29	342.5	0.24
294.2	*0.46*	310.5	*0.36*	326.7	0.28	342.9	0.24
294.6	*0.46*	310.8	*0.36*	327.1	0.28	343.3	0.24
294.9	*0.46*	311.2	*0.36*	327.4	0.28	343.6	0.24
295.3	*0.45*	311.6	*0.36*	327.8	0.28	344.0	0.24
295.7	*0.45*	312.0	*0.35*	328.2	0.28	344.4	0.24
296.0	*0.45*	312.3	*0.35*	328.6	0.27	344.7	0.24
296.4	*0.45*	312.7	*0.35*	328.9	0.27	345.1	0.23
296.8	*0.44*	313.1	*0.35*	329.3	0.27	345.5	0.23
297.1	*0.44*	313.4	*0.35*	329.7	0.27	345.8	0.23
297.5	*0.44*	313.8	*0.34*	330.0	0.27	346.2	0.23
297.9	*0.44*	314.2	*0.34*	330.4	0.26	346.6	0.23
298.3	*0.43*	314.5	*0.34*	330.8	0.27	346.9	0.22
298.6	*0.43*	314.9	*0.34*	331.1	0.26	347.3	0.22
299.0	*0.43*	315.3	*0.34*	331.5	0.26	347.7	0.22
299.4	*0.43*	315.6	*0.34*	331.9	0.26	348.0	0.21
299.7	*0.42*	316.0	*0.33*	332.2	0.27	348.4	0.21
300.1	*0.42*	316.4	*0.33*	332.6	0.27	348.8	0.21
300.5	*0.42*	316.8	*0.33*	333.0	0.26	349.1	0.21
300.9	*0.42*	317.1	*0.33*	333.3	0.27	349.5	0.21
301.2	*0.42*	317.5	*0.33*	333.7	0.27	349.9	0.20
301.6	*0.41*	317.9	*0.32*	334.1	0.27	350.2	0.20
302.0	*0.41*	318.2	*0.32*	334.4	0.27	350.6	0.20
302.3	*0.41*	318.6	*0.32*	334.8	0.26	351.0	0.20
302.7	*0.41*	319.0	*0.32*	335.2	0.26	351.3	0.20
303.1	*0.40*	319.3	*0.32*	335.5	0.26	351.7	0.20
303.4	*0.40*	319.7	*0.32*	335.9	0.26	352.0	0.20
303.8	*0.40*	320.1	0.31	336.3	0.26	352.4	0.19
304.2	*0.40*	320.4	0.31	336.6	0.26	352.8	0.19
304.6	*0.40*	320.8	0.31	337.0	0.25	353.1	0.19
304.9	*0.39*	321.2	0.31	337.4	0.25	353.5	0.19
305.3	*0.39*	321.6	0.31	337.7	0.25	353.9	0.19
305.7	*0.39*	321.9	0.31	338.1	0.25	354.2	0.19

λ	$K_d(\lambda)$	λ	$K_d(\lambda)$	λ	$K_d(\lambda)$	λ	$K_d(\lambda)$
354.6	0.18	372.1	0.15	389.6	0.15	406.9	0.16
355.0	0.18	372.5	0.15	389.9	0.15	407.3	0.16
355.3	0.18	372.9	0.15	390.3	0.15	407.7	0.16
355.7	0.18	373.2	0.15	390.7	0.15	408.0	0.16
356.1	0.18	373.6	0.15	391.0	0.15	408.4	0.16
356.4	0.17	374.0	0.15	391.4	0.15	408.7	0.16
356.8	0.17	374.3	0.15	391.7	0.15	409.1	0.16
357.2	0.17	374.7	0.15	392.1	0.15	409.5	0.16
357.5	0.17	375.0	0.15	392.5	0.15	409.8	0.16
357.9	0.17	375.4	0.15	392.8	0.15	410.2	0.16
358.3	0.17	375.8	0.15	393.2	0.15	410.5	0.16
358.6	0.17	376.1	0.15	393.6	0.15	410.9	0.16
359.0	0.17	376.5	0.15	393.9	0.15	411.3	0.16
359.4	0.16	376.9	0.15	394.3	0.15	411.6	0.16
359.7	0.16	377.2	0.15	394.6	0.15	412.0	0.16
360.1	0.16	377.6	0.15	395.0	0.15	412.3	0.16
360.5	0.16	378.0	0.15	395.4	0.15	412.7	0.16
360.8	0.16	378.3	0.15	395.7	0.15	413.1	0.16
361.2	0.16	378.7	0.16	396.1	0.15	413.4	0.16
361.6	0.16	379.0	0.15	396.5	0.15	413.8	0.16
361.9	0.16	379.4	0.16	396.8	0.15	414.1	0.16
362.3	0.16	379.8	0.16	397.2	0.15	414.5	0.16
362.6	0.16	380.1	0.15	397.5	0.15	414.9	0.17
363.0	0.16	380.5	0.16	397.9	0.15	415.2	0.17
363.4	0.16	380.9	0.15	398.3	0.15	415.6	0.17
363.7	0.16	381.2	0.16	398.6	0.15	415.9	0.17
364.1	0.16	381.6	0.16	399.0	0.15	416.3	0.17
364.5	0.16	382.0	0.16	399.3	0.15	416.7	0.17
364.8	0.16	382.3	0.16	399.7	0.15	417.0	0.17
365.2	0.16	382.7	0.16	400.1	0.15	417.4	0.17
365.6	0.16	383.0	0.16	400.4	0.15	417.7	0.17
365.9	0.16	383.4	0.15	400.8	0.15	418.1	0.17
366.3	0.16	383.8	0.15	401.2	0.15	418.5	0.17
366.7	0.16	384.1	0.15	401.5	0.16	418.8	0.17
367.0	0.16	384.5	0.15	401.9	0.16	419.2	0.17
367.4	0.16	384.9	0.15	402.2	0.16	419.5	0.17
367.8	0.16	385.2	0.15	402.6	0.16	419.9	0.17
368.1	0.16	385.6	0.15	403.0	0.16	420.3	0.17
368.5	0.16	385.9	0.15	403.3	0.16	420.6	0.17
368.9	0.16	386.3	0.15	403.7	0.16	421.0	0.17
369.2	0.16	386.7	0.15	404.0	0.16	421.3	0.17
369.6	0.16	387.0	0.15	404.4	0.16	421.7	0.17
369.9	0.16	387.4	0.16	404.8	0.16	422.1	0.17
370.3	0.15	387.8	0.15	405.1	0.16	422.4	0.17
370.7	0.15	388.1	0.15	405.5	0.16	422.8	0.17
371.0	0.15	388.5	0.15	405.8	0.16	423.1	0.17
371.4	0.15	388.8	0.15	406.2	0.16	423.5	0.17
371.8	0.15	389.2	0.15	406.6	0.16	423.9	0.17

λ	$K_d(\lambda)$	λ	$K_d(\lambda)$	λ	$K_d(\lambda)$	λ	$K_d(\lambda)$
424.2	0.17	441.4	0.17	458.5	0.15	475.5	0.14
424.6	0.17	441.8	0.17	458.9	0.15	475.9	0.14
424.9	0.17	442.1	0.17	459.2	0.15	476.2	0.14
425.3	0.17	442.5	0.17	459.6	0.15	476.6	0.14
425.6	0.17	442.8	0.17	459.9	0.15	476.9	0.13
426.0	0.17	443.2	0.17	460.3	0.15	477.3	0.13
426.4	0.17	443.5	0.17	460.6	0.15	477.7	0.13
426.7	0.17	443.9	0.17	461.0	0.15	478.0	0.13
427.1	0.17	444.3	0.17	461.4	0.15	478.4	0.13
427.4	0.17	444.6	0.17	461.7	0.15	478.7	0.13
427.8	0.17	445.0	0.16	462.1	0.15	479.1	0.13
428.2	0.17	445.3	0.16	462.4	0.15	479.4	0.13
428.5	0.17	445.7	0.16	462.8	0.15	479.8	0.13
428.9	0.17	446.0	0.16	463.1	0.15	480.1	0.13
429.2	0.17	446.4	0.16	463.5	0.15	480.5	0.13
429.6	0.17	446.8	0.16	463.8	0.15	480.8	0.13
430.0	0.17	447.1	0.16	464.2	0.15	481.2	0.13
430.3	0.17	447.5	0.16	464.5	0.15	481.5	0.13
430.7	0.17	447.8	0.16	464.9	0.15	481.9	0.13
431.0	0.17	448.2	0.16	465.3	0.15	482.2	0.13
431.4	0.17	448.5	0.16	465.6	0.15	482.6	0.13
431.7	0.17	448.9	0.16	466.0	0.15	482.9	0.13
432.1	0.17	449.3	0.16	466.3	0.15	483.3	0.13
432.5	0.17	449.6	0.16	466.7	0.15	483.7	0.13
432.8	0.17	450.0	0.16	467.0	0.15	484.0	0.13
433.2	0.17	450.3	0.16	467.4	0.15	484.4	0.13
433.5	0.17	450.7	0.16	467.7	0.15	484.7	0.13
433.9	0.17	451.0	0.16	468.1	0.15	485.1	0.13
434.3	0.17	451.4	0.16	468.5	0.15	485.4	0.13
434.6	0.17	451.8	0.16	468.8	0.15	485.8	0.13
435.0	0.17	452.1	0.16	469.2	0.15	486.1	0.13
435.3	0.17	452.5	0.16	469.5	0.15	486.5	0.13
435.7	0.17	452.8	0.16	469.9	0.14	486.8	0.13
436.0	0.17	453.2	0.16	470.2	0.14	487.2	0.13
436.4	0.17	453.5	0.16	470.6	0.14	487.5	0.13
436.8	0.17	453.9	0.16	470.9	0.14	487.9	0.13
437.1	0.17	454.2	0.16	471.3	0.14	488.2	0.13
437.5	0.17	454.6	0.16	471.6	0.14	488.6	0.13
437.8	0.17	455.0	0.16	472.0	0.14	488.9	0.13
438.2	0.17	455.3	0.16	472.3	0.14	489.3	0.13
438.5	0.17	455.7	0.16	472.7	0.14	489.6	0.13
438.9	0.17	456.0	0.16	473.1	0.14	490.0	0.13
439.3	0.17	456.4	0.16	473.4	0.14	490.3	0.13
439.6	0.17	456.7	0.16	473.8	0.14	490.7	0.13
440.0	0.17	457.1	0.16	474.1	0.14	491.1	0.13
440.3	0.17	457.4	0.16	474.5	0.14	491.4	0.13
440.7	0.17	457.8	0.16	474.8	0.14	491.8	0.13
441.0	0.17	458.2	0.15	475.2	0.14	492.1	0.13

λ	$K_d(\lambda)$	λ	$K_d(\lambda)$	λ	$K_d(\lambda)$	λ	$K_d(\lambda)$
492.5	0.13	509.3	0.12	526.0	0.11	542.7	0.10
492.8	0.13	509.6	0.12	526.4	0.11	543.0	0.10
493.2	0.13	510.0	0.12	526.7	0.11	543.4	0.10
493.5	0.13	510.3	0.12	527.1	0.10	543.7	0.10
493.9	0.13	510.7	0.12	527.4	0.10	544.1	0.10
494.2	0.13	511.0	0.12	527.8	0.10	544.4	0.10
494.6	0.13	511.4	0.12	528.1	0.10	544.8	0.10
494.9	0.13	511.7	0.12	528.5	0.10	545.1	0.10
495.3	0.13	512.1	0.12	528.8	0.10	545.5	0.10
495.6	0.13	512.4	0.12	529.2	0.10	545.8	0.10
496.0	0.13	512.8	0.12	529.5	0.10	546.1	0.10
496.3	0.13	513.1	0.12	529.9	0.10	546.5	0.10
496.7	0.13	513.5	0.12	530.2	0.10	546.8	0.10
497.0	0.13	513.8	0.12	530.6	0.10	547.2	0.10
497.4	0.13	514.2	0.12	530.9	0.10	547.5	0.10
497.7	0.13	514.5	0.12	531.3	0.10	547.9	0.10
498.1	0.13	514.9	0.12	531.6	0.10	548.2	0.10
498.4	0.13	515.2	0.12	531.9	0.10	548.6	0.10
498.8	0.13	515.6	0.12	532.3	0.10	548.9	0.10
499.1	0.12	515.9	0.11	532.6	0.10	549.3	0.10
499.5	0.12	516.3	0.11	533.0	0.10	549.6	0.10
499.8	0.12	516.6	0.11	533.3	0.10	549.9	0.10
500.2	0.12	517.0	0.11	533.7	0.10	550.3	0.10
500.5	0.12	517.3	0.11	534.0	0.10	550.6	0.10
500.9	0.12	517.7	0.11	534.4	0.10	551.0	0.10
501.2	0.12	518.0	0.11	534.7	0.10	551.3	0.10
501.6	0.12	518.4	0.11	535.1	0.10	551.7	0.10
501.9	0.12	518.7	0.11	535.4	0.10	552.0	0.10
502.3	0.12	519.1	0.11	535.8	0.10	552.4	0.10
502.6	0.12	519.4	0.11	536.1	0.10	552.7	0.10
503.0	0.12	519.8	0.11	536.5	0.10	553.0	0.10
503.3	0.12	520.1	0.11	536.8	0.10	553.4	0.10
503.7	0.12	520.5	0.11	537.2	0.10	553.7	0.10
504.0	0.12	520.8	0.11	537.5	0.10	554.1	0.10
504.4	0.12	521.2	0.11	537.8	0.10	554.4	0.10
504.7	0.12	521.5	0.11	538.2	0.10	554.8	0.10
505.1	0.12	521.9	0.11	538.5	0.10	555.1	0.10
505.4	0.12	522.2	0.11	538.9	0.10	555.5	0.10
505.8	0.12	522.6	0.11	539.2	0.10	555.8	0.10
506.1	0.12	522.9	0.11	539.6	0.10	556.1	0.10
506.5	0.12	523.3	0.11	539.9	0.10	556.5	0.10
506.8	0.12	523.6	0.11	540.3	0.10	556.8	0.10
507.2	0.12	524.0	0.11	540.6	0.10	557.2	0.10
507.5	0.12	524.3	0.11	541.0	0.10	557.5	0.10
507.9	0.12	524.6	0.11	541.3	0.10	557.9	0.10
508.2	0.12	525.0	0.11	541.7	0.10	558.2	0.10
508.6	0.12	525.3	0.11	542.0	0.10	558.6	0.10
508.9	0.12	525.7	0.11	542.3	0.10	558.9	0.10

λ	$K_d(\lambda)$	λ	$K_d(\lambda)$	λ	$K_d(\lambda)$	λ	$K_d(\lambda)$
559.2	0.10	575.7	0.11	592.0	0.16	608.3	0.27
559.6	0.10	576.0	0.11	592.4	0.16	608.6	0.27
559.9	0.10	576.4	0.11	592.7	0.17	609.0	0.27
560.3	0.10	576.7	0.11	593.1	0.17	609.3	0.27
560.6	0.10	577.1	0.11	593.4	0.17	609.6	0.27
561.0	0.10	577.4	0.11	593.7	0.17	610.0	0.27
561.3	0.10	577.7	0.11	594.1	0.17	610.3	0.27
561.6	0.10	578.1	0.11	594.4	0.18	610.6	0.27
562.0	0.10	578.4	0.11	594.8	0.18	611.0	0.27
562.3	0.10	578.8	0.11	595.1	0.18	611.3	0.27
562.7	0.10	579.1	0.11	595.4	0.18	611.7	0.27
563.0	0.10	579.4	0.11	595.8	0.19	612.0	0.27
563.4	0.10	579.8	0.12	596.1	0.19	612.3	0.28
563.7	0.10	580.1	0.12	596.5	0.19	612.7	0.28
564.0	0.10	580.5	0.12	596.8	0.19	613.0	0.28
564.4	0.10	580.8	0.12	597.1	0.20	613.3	0.28
564.7	0.10	581.2	0.12	597.5	0.20	613.7	0.28
565.1	0.10	581.5	0.12	597.8	0.20	614.0	0.28
565.4	0.10	581.8	0.12	598.1	0.20	614.4	0.28
565.8	0.10	582.2	0.12	598.5	0.21	614.7	0.28
566.1	0.10	582.5	0.12	598.8	0.21	615.0	0.28
566.4	0.10	582.9	0.13	599.2	0.21	615.4	0.28
566.8	0.10	583.2	0.13	599.5	0.22	615.7	0.29
567.1	0.10	583.5	0.13	599.8	0.22	616.0	0.29
567.5	0.10	583.9	0.13	600.2	0.22	616.4	0.29
567.8	0.10	584.2	0.13	600.5	0.23	616.7	0.29
568.2	0.10	584.6	0.13	600.9	0.23	617.0	0.29
568.5	0.10	584.9	0.13	601.2	0.23	617.4	0.29
568.8	0.10	585.2	0.13	601.5	0.23	617.7	0.29
569.2	0.10	585.6	0.14	601.9	0.24	618.1	0.29
569.5	0.10	585.9	0.14	602.2	0.24	618.4	0.29
569.9	0.10	586.3	0.14	602.5	0.24	618.7	0.29
570.2	0.10	586.6	0.14	602.9	0.24	619.1	0.29
570.6	0.10	586.9	0.14	603.2	0.25	619.4	0.29
570.9	0.10	587.3	0.14	603.6	0.25	619.7	0.30
571.2	0.10	587.6	0.14	603.9	0.25	620.1	0.30
571.6	0.10	588.0	0.15	604.2	0.25	620.4	0.30
571.9	0.10	588.3	0.15	604.6	0.25	620.7	0.30
572.3	0.10	588.6	0.15	604.9	0.25	621.1	0.30
572.6	0.10	589.0	0.15	605.2	0.26	621.4	0.30
573.0	0.10	589.3	0.15	605.6	0.26	621.7	0.30
573.3	0.10	589.7	0.15	605.9	0.26	622.1	0.30
573.6	0.10	590.0	0.15	606.3	0.26	622.4	0.30
574.0	0.10	590.3	0.16	606.6	0.26	622.8	0.30
574.3	0.10	590.7	0.16	606.9	0.26	623.1	0.30
574.7	0.10	591.0	0.16	607.3	0.26	623.4	0.30
575.0	0.11	591.4	0.16	607.6	0.26	623.8	0.30
575.3	0.11	591.7	0.16	608.0	0.26	624.1	0.31

λ	$K_d(\lambda)$	λ	$K_d(\lambda)$	λ	$K_d(\lambda)$	λ	$K_d(\lambda)$
624.4	0.31	640.5	0.34	656.4	0.39	672.2	0.53
624.8	0.31	640.8	0.34	656.7	0.40	672.5	0.52
625.1	0.31	641.1	0.34	657.1	0.40	672.9	0.52
625.4	0.31	641.5	0.34	657.4	0.40	673.2	0.52
625.8	0.31	641.8	0.34	657.7	0.40	673.5	0.53
626.1	0.31	642.1	0.35	658.0	0.41	673.8	0.52
626.4	0.31	642.5	0.35	658.4	0.41	674.2	0.53
626.8	0.31	642.8	0.35	658.7	0.41	674.5	0.53
627.1	0.31	643.1	0.35	659.0	0.42	674.8	0.54
627.4	0.31	643.5	0.35	659.4	0.42	675.2	0.51
627.8	0.32	643.8	0.35	659.7	0.42	675.5	0.55
628.1	0.32	644.1	0.35	660.0	0.42	675.8	0.53
628.4	0.32	644.5	0.35	660.4	0.43	676.1	0.54
628.8	0.32	644.8	0.35	660.7	0.43	676.5	0.54
629.1	0.32	645.1	0.35	661.0	0.43	676.8	0.54
629.5	0.32	645.5	0.35	661.3	0.44	677.1	0.54
629.8	0.32	645.8	0.35	661.7	0.44	677.5	0.54
630.1	0.32	646.1	0.35	662.0	0.44	677.8	0.54
630.5	0.32	646.5	0.35	662.3	0.45	678.1	0.55
630.8	0.32	646.8	0.35	662.7	0.45	678.4	0.54
631.1	0.32	647.1	0.35	663.0	0.45	678.8	0.54
631.5	0.32	647.4	0.36	663.3	0.45	679.1	0.54
631.8	0.33	647.8	0.36	663.7	0.46	679.4	0.56
632.1	0.33	648.1	0.36	664.0	0.46	679.7	0.54
632.5	0.33	648.4	0.36	664.3	0.46	680.1	0.54
632.8	0.33	648.8	0.36	664.6	0.47	680.4	0.54
633.1	0.33	649.1	0.36	665.0	0.47	680.7	0.54
633.5	0.33	649.4	0.36	665.3	0.47	681.1	0.54
633.8	0.33	649.8	0.36	665.6	0.47	681.4	0.53
634.1	0.33	650.1	0.36	666.0	0.47	681.7	0.53
634.5	0.33	650.4	0.36	666.3	0.48	682.0	0.53
634.8	0.33	650.8	0.37	666.6	0.48	682.4	0.52
635.1	0.33	651.1	0.37	666.9	0.49	682.7	0.52
635.5	0.33	651.4	0.37	667.3	0.49	683.0	0.53
635.8	0.33	651.8	0.37	667.6	0.49	683.3	0.53
636.1	0.34	652.1	0.37	667.9	0.49	683.7	0.53
636.5	0.34	652.4	0.37	668.3	0.49	684.0	0.53
636.8	0.34	652.8	0.38	668.6	0.49	684.3	0.53
637.1	0.34	653.1	0.38	668.9	0.49	684.7	0.53
637.5	0.34	653.4	0.38	669.3	0.49	685.0	0.53
637.8	0.34	653.7	0.38	669.6	0.50	685.3	0.52
638.1	0.34	654.1	0.38	669.9	0.50	685.6	0.52
638.5	0.34	654.4	0.38	670.2	0.50	686.0	0.53
638.8	0.34	654.7	0.38	670.6	0.50	686.3	0.53
639.1	0.34	655.1	0.39	670.9	0.51	686.6	0.53
639.5	0.34	655.4	0.39	671.2	0.51	686.9	0.52
639.8	0.34	655.7	0.39	671.6	0.51	687.3	0.52
640.1	0.34	656.1	0.39	671.9	0.51	687.6	0.52

λ	$K_d(\lambda)$	λ	$K_d(\lambda)$	λ	$K_d(\lambda)$	λ	$K_d(\lambda)$
687.9	0.52	690.8	0.52	693.8	0.56	696.7	0.55
688.2	0.52	691.2	0.52	694.1	0.57	697.0	0.56
688.6	0.52	691.5	0.52	694.4	0.56	697.3	0.57
688.9	0.53	691.8	0.53	694.7	0.56	697.7	0.57
689.2	0.53	692.1	0.53	695.1	0.57	698.0	0.57
689.5	0.53	692.5	0.53	695.4	0.57	698.3	0.58
689.9	0.52	692.8	0.53	695.7	0.57	698.6	0.59
690.2	0.52	693.1	0.54	696.0	0.57	699.0	0.59
690.5	0.52	693.4	0.55	696.4	0.55	699.3	0.60

$K_d(\lambda)$ for 320-700 nm were determined from *in situ* measurements of downwelling irradiance according to Eq. A.1. Instrumentation, the study site, and data acquisition conditions are described in Section 2.2 of the main text. The data in this table are available online at https://doi.org/10.1594/PANGAEA.879578.

[a] Due the low signal-to-noise ratio of the Jaz irradiance data in the UVB band, $K_d(\lambda)$ for 290-320 nm (values *in italics*) were estimated using an exponential model ($K_d = e^{-0.0149\lambda+3.60}$) fit to values from the 320-370 nm interval.

Table A4
Hydrolysis of fluorogenic substrates used to monitor bacterial exoenzyme activities during the 14 December 2013 liposome photooxidation experiment.

Timepoint	4-MUF-butyrate[a] (nmol L^{-1} hr^{-1} ± SE)		leu-MCA[b] (nmol L^{-1} hr^{-1} ± SE)	
	Control (dark) + het. bact.	+ UVR + het. bact.	Control (dark) + het. bact.	+ UVR + het. bact.
1340	187 ± 6	176 ± 21	3.7 ± 0.5	3.1 ± 0.4
1750	140 ± 10	217 ± 25	4.3 ± 0.8	3.1 ± 1.1

Activities reported as mean ± SE (n = 3). Hydrolysis of the two other added substrates (4-MUF-alpha-D-glucopyranoside and 4-MUF-PO_4) could not be detected.
[a] 4-methylumbelliferone-butyrate-heptanoate-palmitate; hydrolysis monitored as proxy for lipase activity
[b] L-Leucine-4-methylcoumaryl-7-amide; hydrolysis monitored as proxy for aminopeptidase activity

Table A5
Identification of chromatographic peak area in a particulate marine lipid sample from the West Antarctic Peninsula.

	Peak area $\times 10^9$	Fraction total chrom. peak area	Fraction total putatively identified lipids	Fraction positively identified, unoxidized lipids	No. unique HPLC-MS features represented[a]
Total peak area, *m/z* 200-1500	153	1.00	–	–	21,839
All lipids putatively identified using LOBSTAHS[b]	72	0.47	1.00	–	2,298
Unoxidized lipids positively identified using multiple screening criteria[c]				1.00	
Unoxidized IP-DAG	7.8	0.05	0.11	0.12	
Photosynthetic pigments	3.1	0.02	0.04	0.05	
Unoxidized TAG	55	0.36	0.77	0.83	
DNPPE (internal standard)	0.4	< 0.01	0.01	0.01	
Other[d]	5.4	0.04	0.07		

Data in this table are presented for the water column sample shown in the leftmost position in Fig. 7 and Fig. 8; the corresponding chromatogram is presented in Fig. A8. HPLC-ESI-MS analysis and subsequent identification and screening of lipids were performed as described in the main text.

[a] Equivalent to number of xcms peakgroups.

[b] See Section 2.5.1 in the main text. A full list of the LOBSTAHS compound assignments applied to the data can be downloaded from https://github.com/jamesrco/LipidPhotoOxBox/blob/master/data/nice/LOBSTAHS_lipid_identities/PAL1314_LMG1401_particulate_all_LOBSTAHS_IDs_pos.csv (sample "QE003120").

[c] Section 2.5.1 in the main text describes the additional screening criteria. The list of final, high-confidence IP-DAG identified in the sample (n = 318; abundances in units of pmol L^{-1}) is contained in https://github.com/jamesrco/LipidPhotoOxBox/blob/master/data/nice/LOBSTAHS_lipid_identities/PAL1314_LMG1401_particulate_IP-DAG_pmol_L.final.csv or https://doi.org/10.1594/PANGAEA.879618.

[d] Includes oxidized lipids, oxylipins, lyso lipids, and low-confidence compound assignments of unoxidized species.

References

Benton, H.P., Want, E.J. and Ebbels, T.M.D. (2010) Correction of mass calibration gaps in liquid chromatography-mass spectrometry metabolomics data. *Bioinformatics* **26**, 2488-2489.

Brosnan, I.G. (2015) Calibration and data processing Biospherical C-OPS system used during the Ocean Optics 2015 class cruise. Document Version 1.0. NASA Ames Research Center, Moffett Field, CA. 9 pp.

Collins, J.R., Edwards, B.R., Fredricks, H.F. and Van Mooy, B.A.S. (2016) LOBSTAHS: An adduct-based lipidomics strategy for discovery and identification of oxidative stress biomarkers. *Anal. Chem.* **88**, 7154-7162.

Crastes de Paulet, A., Douste-Blazy, L. and Paoletti, R. (1988) *Free Radicals, Lipoproteins, and Membrane Lipids*. Plenum Publishing Corporation, New York. 407 pp.

Desharnais, B., Camirand-Lemyre, F., Mireault, P. and Skinner, C.D. (2015) Determination of confidence intervals in non-normal data: Application of the bootstrap to cocaine concentration in femoral blood. *J. Anal. Toxicol.* **39**, 113-117.

Edwards, B.R., Reddy, C.M., Camilli, R., Carmichael, C.A., Longnecker, K. and Van Mooy, B.A.S. (2011) Rapid microbial respiration of oil from the Deepwater Horizon spill in offshore surface waters of the Gulf of Mexico. *Environmental Research Letters* **6**.

Hu, C., Muller-Karger, F.E. and Zepp, R.G. (2002) Absorbance, absorption coefficient, and apparent quantum yield: A comment on common ambiguity in the use of these optical concepts. *Limnol. Oceanogr.* **47**, 1261-1267.

Jankowski, J.J., Kieber, D.J. and Mopper, K. (1999) Nitrate and nitrite ultraviolet actinometers. *Photochem. Photobiol.* **70**, 319-328.

Kessner, D., Chambers, M., Burke, R., Agus, D. and Mallick, P. (2008) ProteoWizard: open source software for rapid proteomics tools development. *Bioinformatics* **24**, 2534–2536.

Kieber, D.J., Toole, D.A., Jankowski, J.J., Kiene, R.P., Westby, G.R., del Valle, D.A. and Slezak, D. (2007) Chemical "light meters" for photochemical and photobiological studies. *Aquat. Sci.* **69**, 360-376.

Kuhl, C., Tautenhahn, R., Bottcher, C., Larson, T.R. and Neumann, S. (2012) CAMERA: an integrated strategy for compound spectra extraction and annotation of liquid chromatography/mass spectrometry data sets. *Anal. Chem.* **84**, 283-289.

Levitus, S. (1982) *Climatological Atlas of the World Ocean*. NOAA/ERL GFDL Professional Paper 13.

McHowat, J., Jones, J.H. and Creer, M.H. (1996) Quantitation of individual phospholipid molecular species by UV absorption measurements. *J. Lipid Res.* **37**, 2450-2460.

Miller, W.L. (1998) Effects of UV radiation on aquatic humus: Photochemical principles and experimental considerations. In *Aquatic Humic Substances: Ecology and Biogeochemistry* (eds. D.O. Hessen and L.J. Tranvik). Springer Berlin Heidelberg, Berlin, Heidelberg. pp. 125-143.

Morrow, J.H., Booth, C.R., Lind, R.N. and Hooker, S.B. (2010) The Compact Optical Profiling System (C-OPS). In *Advances in Measuring the Apparent Optical Properties (AOPs) of Optically Complex Waters,* NASA Tech. Memo. 2010–215856 (eds. J.H. Morrow, S.B. Hooker, C.R. Booth, G. Bernhard, R.N. Lind and J.W. Brown). NASA Goddard Space Flight Center, Greenbelt, Maryland. pp. 42-50.

Popendorf, K.J., Fredricks, H.F. and Van Mooy, B.A.S. (2013) Molecular ion-independent quantification of polar glycerolipid classes in marine plankton using triple quadrupole MS. *Lipids* **48**, 185-195.

R Core Team (2016) R: a language and environment for statistical computing, version 3.4.0. R Foundation for Statistical Computing, Vienna, Austria.

Rontani, J.-F., Belt, S.T., Brown, T.A., Amiraux, R., Gosselin, M., Vaultier, F. and Mundy, C.J. (2016) Monitoring abiotic degradation in sinking versus suspended Arctic sea ice algae during a spring ice melt using specific lipid oxidation tracers. *Org. Geochem.* **98**, 82-97.

Smith, C.A., Want, E.J., O'Maille, G., Abagyan, R. and Siuzdak, G. (2006) XCMS: processing mass spectrometry data for metabolite profiling using nonlinear peak alignment, matching, and identification. *Anal. Chem.* **78**, 779–787.

Spector, M.S., Easwaran, K.R.K., Jyothi, G., Selinger, J.V., Singh, A. and Schnur, J.M. (1996) Chiral molecular self-assembly of phospholipid tubules: A circular dichroism study. *Proceedings of the National Academy of Sciences of the United States of America* **93**, 12943-12946.

Sumner, L., Amberg, A., Barrett, D., Beale, M., Beger, R. and Daykin, C. (2007) Proposed minimum reporting standards for chemical analysis. *Metabolomics* **3**, 211–221.

Tautenhahn, R., Boettcher, C. and Neumann, S. (2008) Highly sensitive feature detection for high resolution LC/MS. *BMC Bioinformatics* **9**, 504.

Thomas, C.P., Morgan, L.T., Maskrey, B.H., Murphy, R.C., Kühn, H., Hazen, S.L., Goodall, A.H., Hamali, H.A., Collins, P.W. and O'Donnell, V.B. (2010) Phospholipid-esterified eicosanoids are generated in agonist-activated human platelets and enhance tissue factor-dependent thrombin generation. *J. Biol. Chem.* **285**, 6891-6903.

Vähätalo, A.V., Salkinoja-Salonen, M., Taalas, P. and Salonen, K. (2000) Spectrum of the quantum yield for photochemical mineralization of dissolved organic carbon in a humic lake. *Limnol. Oceanogr.* **45**, 664-676.

Van Mooy, B.A.S. and Fredricks, H.F. (2010) Bacterial and eukaryotic intact polar lipids in the eastern subtropical South Pacific: Water-column distribution, planktonic sources, and fatty acid composition. *Geochim. Cosmochim. Acta* **74**, 6499-6516.

Wagner, B.A., Buettner, G.R. and Burns, C.P. (1994) Free radical-mediated lipid peroxidation in cells: Oxidizability is a function of cell lipid *bis*-allylic hydrogen content. *Biochemistry* **33**, 4449-4453.

Whitcutt, J.M. (1957) South African pilchard oil. 6. The isolation and structure of a docosahexaenoic acid from South African pilchard oil. *Biochem. J* **67**, 60-64.

Yao, A.A., Coulibaly, I., Lognay, G., Fauconnier, M.-L. and Thonart, P. (2008) Impact of polyunsaturated fatty acid degradation on survival and acidification activity of freeze-dried *Weissella paramesenteroides* LC11 during storage. *Appl. Microbiol. Biotechnol.* **79**, 1045-1052.

Zhou, F., Liu, S., Hu, Z., Kuang, T., Paulsen, H. and Yang, C. (2009) Effect of monogalactosyldiacylglycerol on the interaction between photosystem II core complex and its antenna complexes in liposomes of thylakoid lipids. *Photosynth. Res.* **99**, 185-193. Levitus, S. (1982) *Climatological Atlas of the World Ocean*. NOAA/ERL GFDL Professional Paper 13.